UNIVERSITY OF THESSALY

SCHOOL OF ENGINEERING

DEPARTMENT OF MECHANICAL ENGINEERING

NITRIDING OF Si-W-Al CAST IRONS

BY:

GEORGIOS BALAMOTIS

TATIANI TSIARA

Submitted in partial fulfillment of the requirements for the degree of Diploma in Mechanical Engineering at the University of Thessaly

Volos, 2025

UNIVERSITY OF THESSALY

SCHOOL OF ENGINEERING

DEPARTMENT OF MECHANICAL ENGINEERING

LABORATORY OF MATERIALS

NITRIDING OF Si-W-Al CAST IRONS

BY:

GEORGIOS BALAMOTIS

TATIANI TSIARA

Submitted in partial fulfillment of the requirements for the degree of Diploma in Mechanical Engineering at the University of Thessaly

Volos, 2025

Approved by the Committee on Final Examination:

Thesis Supervisor: Dr. Eleni Kamoutsi
Laboratory Teaching Staff
Department of Mechanical Engineering
University of Thessaly

Second Examiner: Dr. Gregory Haidemenopoulos
Professor of Physical Metallurgy
Department of Mechanical Engineering
University of Thessaly

Third Examiner: Dr. Emmanouil Bouzakis
Associate Professor of Manufacturing Processes
Department of Mechanical Engineering
University of Thessaly

NITRIDING OF Si - W – Al CAST IRONS

GEORGIOS BALAMOTIS

TATIANI TSIARA

Department of Mechanical Engineering, University of Thessaly

Supervisor: Dr. Eleni Kamoutsi

Abstract

The subject of the present thesis is the thermodynamic calculations and the kinetic simulations of ductile cast iron with the following composition: Fe- 3.5%C-4%Si-1%W-x %Al, when subjected to gas nitriding. The weight percentage of aluminum is selected as 0%, 1%, 2%, 3% and 4%, with the purpose of examining the influence of aluminum addition. Nitriding process is applied to automotive industry to enhance surface properties such as hardness, wear and corrosion resistance. Furthermore, mechanical properties such as fatigue resistance seem to be augmented. The thermodynamic calculations are performed using Thermo- Calc software, utilizing its graphic mode. The results extruded from the calculations are the phase diagrams and the phase fractions. Although, the thermodynamics predict the formation of Si_3N_4 phase, the kinetics and the experimental data suggest neglecting it. Therefore, the phase diagrams are calculated both with and without Si_3N_4 and in the phase fractions it is completely suspended. Aluminum addition expanded both nitrides (γ' and ε) and ferrite to higher nitrogen levels. Other than that, as aluminum content increases the amount of AlN phase seems to be higher. A single point equilibrium is calculated at the specific nitriding temperature to examine the dispersed phases in the ferritic matrix lattice and their compositions. The next step is the simulation of the diffusion that takes place in the diffusion zone. Following the thermodynamic results the kinetics of nitriding are simulated with Dictra module of Thermo-Calc software. At this stage the parameters of diffusion are nitrogen's activity, the nitriding temperature and the duration of the process. Activity is set as the lower boundary of the diffusion and the values under examination are act(N)=100 and act(N)=500. With respect to the temperature, a temperature delta of 10°C is examined. The nitriding duration is 40 hours according to the experimental data and an intermediate duration of 12 hours is also examined.

The aim of this thesis is to understand both the thermodynamics and kinetics of ductile cast iron nitriding. This study is of significant importance for the development of novel materials suitable for industrial applications, such as exhaust manifold design.

Table of Contents

List of Figures

List of Tables

Chapter 1 : Introduction

1.1 Background

Industrial, transportation, and infrastructure development has significantly increased over the past century. Diesel engines play a leading part in these fields because of the advantages they offer over other types of engines, some of them being cost-effectiveness, reliability, power output [1]. However, the proliferation of their use along with the environmental effects have led regulatory authorities to introduce legislation to control emissions and increase fuel efficiency.

Emissions standards, e.g. Euro 7, aiming to reduce nitrogen oxides, carbon monoxide and particulate matter, result in the implementation of technologies such as DPF regeneration, SCR, and EGR. [2]. Moreover, there is a trend to downsize the engines and boost pressure through turbocharging to improve fuel efficiency while new alternative fuels are being introduced. These factors lead to an overall increase in operating temperatures with the augmented thermal load mostly affecting the exhaust manifold, as well as a more corrosive working environment of the exhaust components downstream the combustion chamber.

Exhaust and Turbo Manifolds are made of ductile cast iron due to their advantages, discussed in greater detail in a subsequent chapter. Their subjection to ever-increasing loads in a corrosive environment demands the enhancement of their thermomechanical properties.

Figure 1.1.1:Diesel Turbo Manifold Package - Dodge 6.7L Cummins 2007.5-2012

1.2 Ductile Cast Irons

Cast irons are a widespread engineering material with many applications in the industry. Being an ecomaterial and very cost effective are often used for structural purposes because

they have similar properties with steel, but they are much easier to cast. One of the drawbacks is the brittle nature of the material, especially near the 673 K temperature. The earliest form, gray cast iron, needed days of heat treatment to become ductile.

Ductile Cast Iron is a material with 3.0-4.0wt% of carbon content and high Silicon addition. The difference in the microstructure, though, is crucial and impacts the performance of the material to a large extent. The matrix structure can be ferritic, pearlitic, bainitic or martensitic with dispersed spheroidal graphite and this microstructure is influenced by alloy composition, heat treatment and cooling process. Ferritic ductile cast iron appears to have the best ductility due to the stability of the ferritic phase to a temperature of 600°C.

Their properties such as high strength, durability, oxidation and wear resistance even under corrosive conditions make them the best candidate for many uses in the automotive industry. Gears, pinions, crankshafts are usually made of ductile cast iron. This material also meets standards for thermal and mechanical fatigue resistance so it is used to make brake discs and exhaust manifolds as operation temperatures in such components can reach up to 1000°C even more. [3][4]

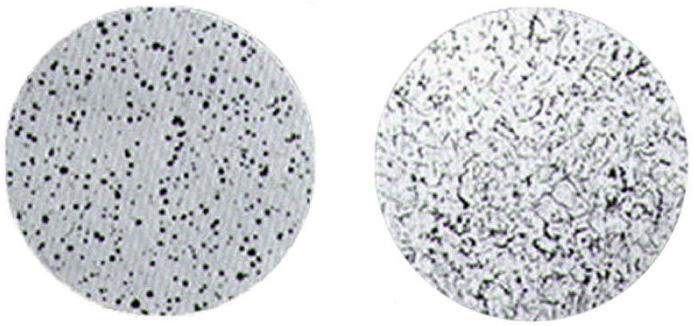

Figure 1.2.1 Microstructure of Ductile Cast Iron (left) and microstructure of Gray Cast Iron (right)

1.3 Material Trends

Exhaust manifolds nowadays are made of Titanium, Stainless Steel or Cast Iron. Titanium, due to its thermal insulation properties, when used, can keep the rest of the engine components relatively cool from the exhaust gases heat. Also, known for its high stiffness to weight ratio, it makes the best candidate for motorsport applications where lightweight and durable components are required. Following, Stainless Steel exhaust manifolds, with slightly inferior properties, are used to modified vehicles to enhance performance. However, fabrication costs make both materials inappropriate for mass production vehicles. [5]

Trading cost with thermomechanical properties automotive manufacturers choose to make the turbo manifolds for their diesel engines of Ductile Cast Iron as weight plays a minor role on everyday cars and heavy vehicles with this type of engine. Consequently, there is a focus on making Ductile Cast Iron more durable against the hot and corrosive environment they operate. To achieve that, new alloys are studied about their properties. Most of them concern the addition of alloying metals to the base Fe-C-Si composition of the cast iron. Currently, SiMo Cast Irons are the most used material, and many researchers study the effect of altering alloying elements and percentages. For example, the influence of Ni and Cr addition is studied having some interesting results.[6][7] Other metal additions concern Al and Nb in various compositions. [8][9][10] Generally, among others, Mn, Cu, Ti, V, W are also candidates for Cast Iron alloying. [7]

Like any other metallic component, as mentioned above, properties are not solely a result of composition. Heat treatment and cooling process impact the final component equally, driving many researchers to study their effects. Alloying elements are also added to boost the nitriding of exhaust manifolds, the last process an exhaust manifold undergoes before it is ready for assembly. This process increases hardness and wear resistance with the creation of phases containing Nitrogen. [11]

1.4 Thesis subject

This thesis aims to contribute to the development of the material with a focus on the nitriding process. As discussed earlier and analyzed in more detail in the following sections, nitriding of the cast irons is a critical process to confer strength, durability and corrosion resistance, being influenced by many factors. Therefore, this thesis attempts to help the comprehension of the nitriding mechanism by studying the existing literature. Additionally, composition of material and constitution of each phase is approached through thermodynamic calculations while studying the effect of aluminum (Al) addition in alloy. Finally, using computational kinetics simulations, the overarching objective of this project is to generate data of the Nitrogen profile as well as phase fractions resulting from the diffusion of the Nitrogen at 510°C and examine sensitivity analysis of time, temperature and Al addition.

Chapter 2 : Nitriding Process

2.1 Nitriding Literature Review

Nitriding of ductile cast irons, as mentioned above, plays a major role in the automotive industry, especially when it comes to exhaust manifold design. Due to the high temperatures of the exhaust, it is important to select such materials that can operate under extreme conditions.

The nitriding procedure is a widespread thermochemical heat treatment included in surface engineering. By the term surface engineering, every method that improves materials' surface for protection in very aggressive environments is described. A major benefit of nitriding that makes the process stand out is that it can be applied to both cast iron and steel (alloy, stainless and tool steel).

There are plenty of methods for nitriding, although the most commonly used are the following [12]:

- Gas Nitriding
- Plasma Nitriding
- Salt bath Nitriding

The standard nitriding temperature range lies between 500°C and 550°C depending on the material and the selected nitriding method. Normally, salt bath nitriding requires a slightly higher temperature.

2.1.1 Gas Nitriding

Gas nitriding is the most optimal surface hardening process for automotive industries, and it can be divided into three distinct stages: heating, nitriding and cooling. The key parameters to control are the gas flow rate, the nitriding temperature and the time of nitriding. The procedure typically lasts between 20 and 70 hours and the duration of exposure to the ammonia environment influences the depth of nitrogen penetration. *Figure 2.1.1* illustrates the stages of gas nitriding by plotting temperature vs time.

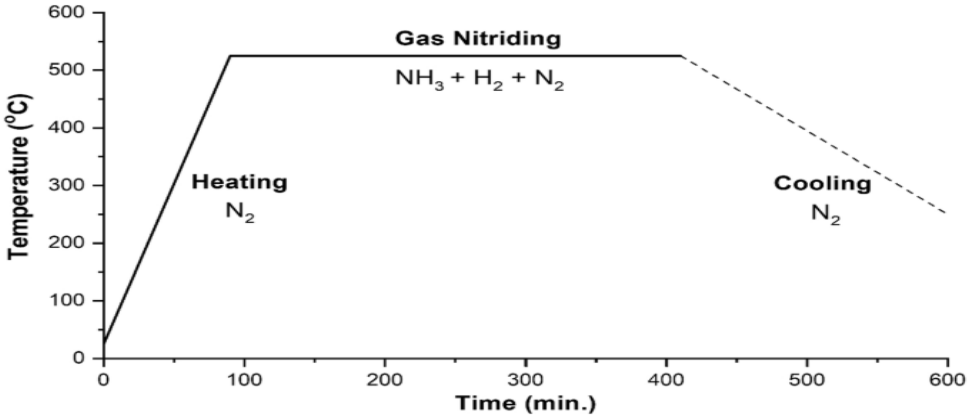

Figure 2.1.1 : The three stages of Gas Nitriding [14]

Initially, the workpiece is positioned inside the furnace, where the temperature gradually increases until the specified nitriding temperature. *Figure 2.1.2* depicts an industrial furnace suitable for gas nitriding technique.

Figure 2.1.2 : Example of a Furnace for Gas Nitriding

The basic chemical reaction that takes place when nitriding is ammonia decomposition, described by the following equation:

$$NH_3 \leftrightarrow N + \frac{3}{2}H_2 \quad \{2.1\}$$

Upon reaching the temperature, ammonia in gaseous form undergoes thermal decomposition according to the previous chemical equation. Atomic nitrogen starts to diffuse into the surface and simultaneously starts to react with the alloying elements of the cast iron. Consequently, nitrides begin to form as dispersed phases in the main ferritic lattice.

In the final stage, the temperature gradually decreases, and the workpiece is removed from the furnace. [13] [14]

During nitriding of cast irons, two layers are formed: the Compound Layer and the Diffusion Zone.[15] A simple schematic representation of the layers is depicted in *Figure 3.3.6.*

The Compound Layer (White Layer) is enriched with nitrogen and because of the high nitrogen concentration, the phases formed are: ε nitride and γ′ nitride in accordance with the thermodynamic results. Due to the presence of the nitrides, compound layer creates a strong outer surface characterized by high wear and corrosion resistance.

The Diffusion Zone forms after the compound layer and constitutes the region where the diffusion of nitrogen takes place. Nitrogen begins to react with the alloying elements of the cast iron (Al, Si, W) resulting in the formation of stable nitrides. According to the thermodynamics of nitriding the expected nitrides to form are the following: γ′-Fe4N and AlN.

Advantages and Disadvantages of Gas Nitriding

Gas nitriding application offers several advantages. One of them is the relatively low temperatures that nitriding takes place which causes minimal dimensional changes. Subsequently, finish grinding of the workpieces is typically not required.

A major drawback of gas nitriding is the duration of the method that lies between 20 and 70 hours. Furthermore, the use of an ammonia environment presents safety concerns.

2.1.2 Plasma Nitriding

Plasma Nitriding, also known as ion nitriding, is a widespread diffusion process for surface engineering. Plasma can be defined as an ionized gas that combines gaseous and liquid properties.

A schematic representation of plasma nitriding equipment is depicted in *Figure 2.1.3*

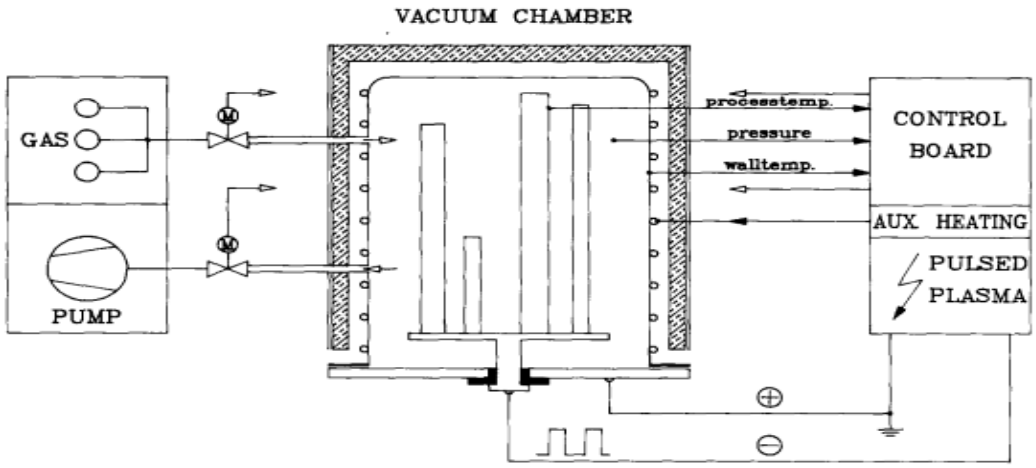

Figure 2.1.3 : Plasma Nitriding Equipment [16]

The mandatory equipment for plasma nitriding is:

- A vacuum chamber where nitriding of the parts takes place. The part is estimated as the cathode.
- A pumping system to reach the required pressure.
- A gas supply for nitrogen that contains gases: Nitrogen, Ammonia, or Hydrogen – Nitrogen mixture.
- Valves between gas supply/pumping system and the vacuum chamber.
- Two electric power supplies: the first one operates with high voltage to create plasma, and the second one is responsible for heating the inner walls of the vacuum chamber.
- A control board that manages parameters of the entire system.

Glow discharge plasma is formed when current passes through gas and a luminous glow is observed. Because of the glow discharge nitrogen can penetrate the surface and start to diffuse into the steel. [16]

A study about plasma nitriding on steels [17], showed that frequently both the compound layer and the diffusion zone are formed.

Advantages and Disadvantages of Plasma Nitriding Method [16]

A key advantage of plasma nitriding is the precise control over the nitrogen-to- hydrogen ratio, which directly influences the thickness of the compound zone responsible for enhancing the wear resistance of the workpiece. Furthermore, plasma nitriding is well-suited for treating complex geometries, including parts requiring selective or partial surface treatment.

The plasma nitriding equipment, as shown in *Figure 2.1.3*, comprises multiple components and devices, making the process more complex to operate and requiring highly skilled operators.

2.1.3 Salt Bath Nitriding

Examining salt bath nitriding, the parts are placed in a salt bath that contains cyanide or cyanate salts (Potassium Cyanite / Sodium Cyanite). Initially, the salts need to be heated to the required temperature. When heat is supplied, salts due to their tendency to melt are in a liquid state. As a result, nitrogen starts to diffuse into the material's surface.

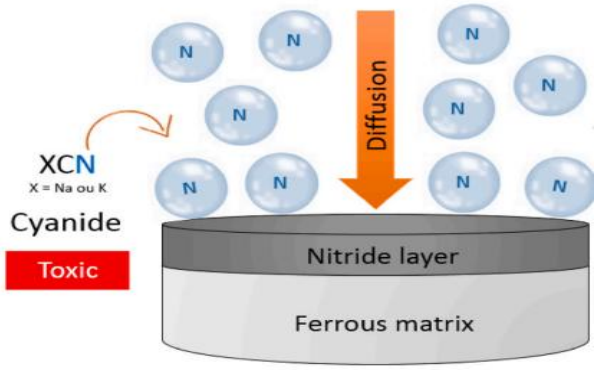

Figure 2.1.4: Schematic illustration of Salt Bath Method, conventional method of using cyanides [18]

Advantages and Disadvantages of Salt Bath Nitriding Method

According to the literature, salt bath nitriding application offers several advantages. Firstly, the process is cost-effective due to low operating and maintenance costs. Additionally, the simplicity of this nitriding method requires a lower skill level for operation.

Although, the major drawback of salt bath nitriding is the toxicity associated with cyanide and cyanate salts that are harmful both for the environment and human health. [18]

2.2 Nitriding Potential K_N and Activity of Nitrogen a_N

When nitriding is selected as surface heat treatment it is essential to evaluate the thickness of the compound zone and the diffusion layer and depth that nitrogen penetrates. There are two crucial parameters that affect the whole nitriding process. These parameters are the Nitriding Potential and the Activity of Nitrogen. [19]

In the gas nitriding method, the fundamental chemical reaction involved, as mentioned above, is the decomposition of ammonia {2.1}. Each chemical reaction is accompanied by a temperature dependent equilibrium constant. For chemical reaction {2.1} that constant is denoted as K_1.

The Nitriding Potential, K_N, indicates the level of nascent nitrogen available for diffusion during nitriding process. The value of K_N is correlated with the chemical composition of the compound layer. The formula that calculates the Nitriding Potential is the following:

$$K_N = \frac{p_{NH_3}}{(p_{H_2})^{\frac{3}{2}}} \quad \{2.2\}$$

where p_{NH_3} and p_{H_2} are partial pressures of ammonia and hydrogen respectively.

Activity of Nitrogen describes the ability of nitrogen to react with the alloying elements and affects nitrogen's diffusion and subsequently the depth that nitrogen penetrates. Activity can be calculated from the following equation, at a pressure of 1 bar:

$$a_N = K_1 K_N \quad \{2.3\}$$

2.3 Nitriding Process of the thesis

Due to the environment restrictions and the need for materials that can operate under extreme conditions such as exhaust manifolds, SiW ductile cast irons were developed.

A study carried out by Kocaeli University in collaboration with University of Thessaly (Laboratory of High Temperature Materials, Kocaeli – Laboratory of Materials, Volos) and presented at the 4th International Symposium on Characterization, showed that the development of SiW cast irons can serve an ideal alternative. [20]

In order to enhance the properties of the material such as wear, fatigue and oxidation resistance the material was subjected to Gas Nitriding. As mentioned above, gas nitriding is a surface treatment that is affected by several parameters, one of which is the duration of the process. Therefore, the study was focused on the impact that had the duration of nitriding to the microstructure and to formation of the Compound Layer and the Diffusion Zone.

Initially, the casting process of the material was performed by using cast- sanding method, followed by nitriding. The samples were positioned into a furnace until the temperature reached 510°C. Simultaneously, the ammonia flow rate was set at $2.5\ \frac{m^3}{h}$. The samples were subjected to nitriding for 12 and 40 hours.

After the nitriding process was completed, the microstructural analysis was performed. The analysis was based on three studies:

- The surface and subsurface components were examined using an X-ray diffractometer (XRD).
- For both surface and cross-sectional examinations, a scanning electron microscope (SEM) was used.
- An energy-dispersive X-ray (EDS) spectrometer was used to determine the chemical compositions of microstructural components.

The results are illustrated in the following figures:

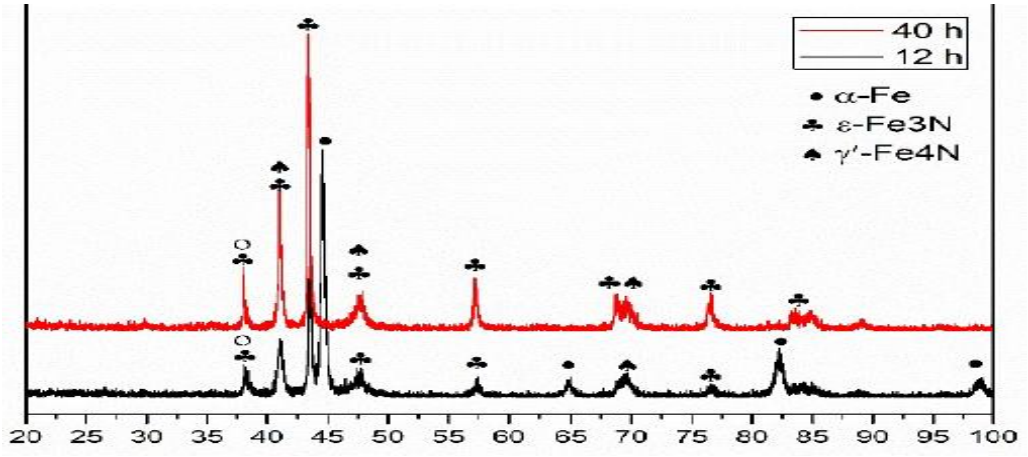

Figure 2.3.1 : XRD patterns of nitrided SiW ductile cast irons [20]

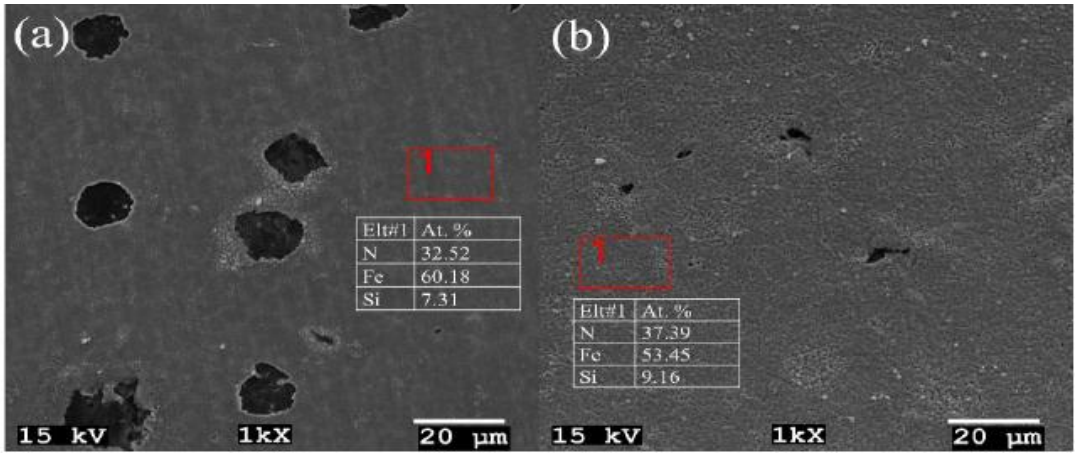

Figure 2.3.2 : SEM images of the surface and EDS analysis results of the SiW for (a) 12 hours and (b) 40 hours [20]

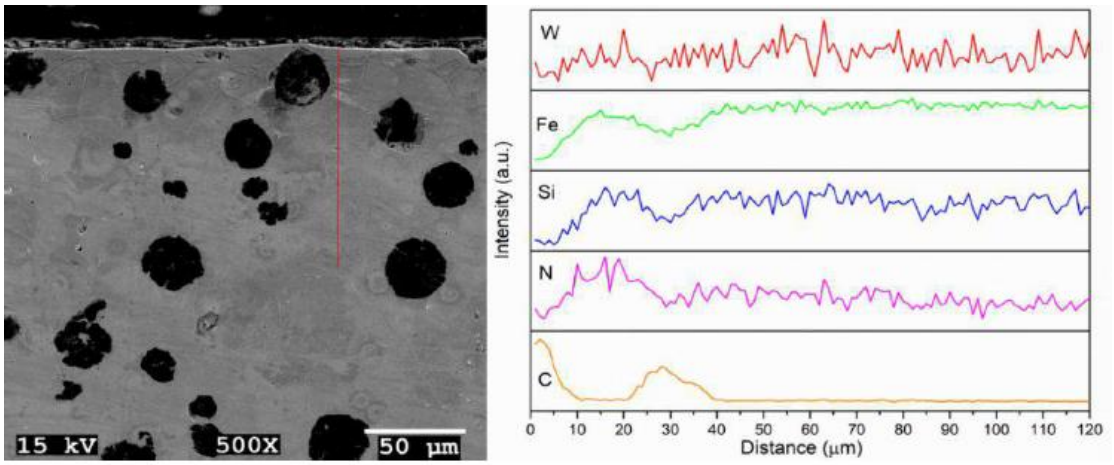

Figure 2.3.3 : SEM image of the cross section of SiW ductile cast iron subjected to 12 hours of nitriding and the elemental distribution as a function of distance [20]

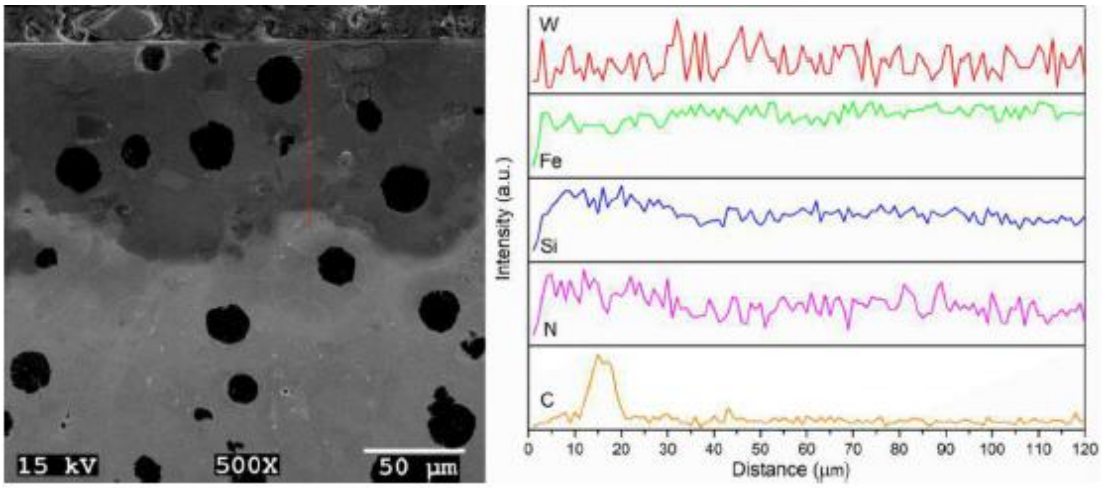

Figure 2.3.4 : SEM image of the cross section of SiW ductile cast iron subjected to 40 hours of nitriding and the elemental distribution as a function of distance [20]

2.4 Material under Examination

The material under examination for the present thesis was a novel ductile cast iron, classified as part of SiW ductile cast irons. More precisely, the composition of the cast iron was the following: Fe – 3.5%C- 4% Si- 1%W – (0-4) % Al. A study that was conducted from Çelik, Haidemenopoulos et al showed that the value of A_1 temperature is crucial to enhance thermal and mechanical properties of the ductile cast iron. Higher values of A_1 temperature can be achieved through the addition of certain alloying elements. The alloying elements are the following: Silicon (Si), Aluminum (Al), Titanium (Ti), Niobium (Nb) and Tungsten (W). Silicon and Aluminum are known as ferrite stabilizers and shift the eutectoid temperature to higher values.

Additionally, aluminum enhances oxidation resistance by forming a stabilized oxide layer. The remaining elements Titanium, Niobium and Tungsten contribute to mechanical properties through the formation of carbides. [21]

Chapter 3 : Thermodynamic Calculations

3.1 CALPHAD Method

Thermodynamic Equilibrium is required to first-approach the problem and acquire the fundamental knowledge about the process studied. Before setting any parameters to simulate the diffusion, there must be basic understanding of the materials and the transformations that may occur. These calculations are conducted with the CALPHAD method. The CALPHAD method, which stands for CALculation of PHAse Diagrams, relies on a computer program combined with databases containing experimental data of binary and ternary systems used to calculate higher order systems. This method can be broken down into four stages :

- Model evaluation on Unary and binary systems
- Experimental evaluation of thermodynamic properties on Ternary and Quaternary systems
- Evaluation of unknown quantities required for free energy description
- Development of free energy models for higher order systems

The stable phases of thermodynamic equilibrium in multiphase systems are given by minimizing the molar Gibbs energy of the system according to [22]:

$$G = \sum_{\varphi} n^{\varphi} G_m^{\varphi} = minimum, \quad \{3.1\}$$

The mathematical model the method uses is out of this thesis' scope and shall not be further discussed.

THERMOCALC software, providing a program using the method discussed above and the corresponding databases for a large variety of potential alloying elements, comprise a useful tool to obtain computational information about materials avoiding possible time and cost barriers that may emerge from an experiment.

3.2 Thermodynamic Equilibrium

For the thermodynamic computations, graphic mode of THERMOCALC software was used where the following parameters were set:

- Composition: Fe - 3.5 C - 4.0 Si – 1W – (0-4wt.%) Al - N
- Temperature: 783K
- Pressure: 1bar
- Database: TCFE14

To calculate the equilibrium calculations N content was set as an independent variable and every phase was suspended. Then, the following phases expected to appear were restored:

1. α – ferritic phase (BCC)
2. γ – austenitic phase (FCC)
3. Liquid phase (L)
4. Cementite phase
5. Graphite Phase (G)
6. ε – nitride phase (HCP)
7. γ' - nitride phase(Fe_4N)

8. κ – carbide phase (KAPPA) / Al-rich carbide
9. AlN phase
10. M_6C phase / W-rich carbide
11. Si_3N_4 phase

3.3 Phase Diagrams

Phase diagrams are 2-D plots where the vertical axis (y) represents the temperature and horizontal axis (x) denotes the content of an alloying element. The following phase diagrams' (y) axis has a range from 300 K to 1000 K, while its (x) axis concerns the N wt.% (weight percent) with a span up to 13wt.%. The calculations were done with the parameters above, but now temperature is also set as a second independent variable. The calculations were repeated for Al wt. content of 0%, 1%, 2%, 3% and 4%.

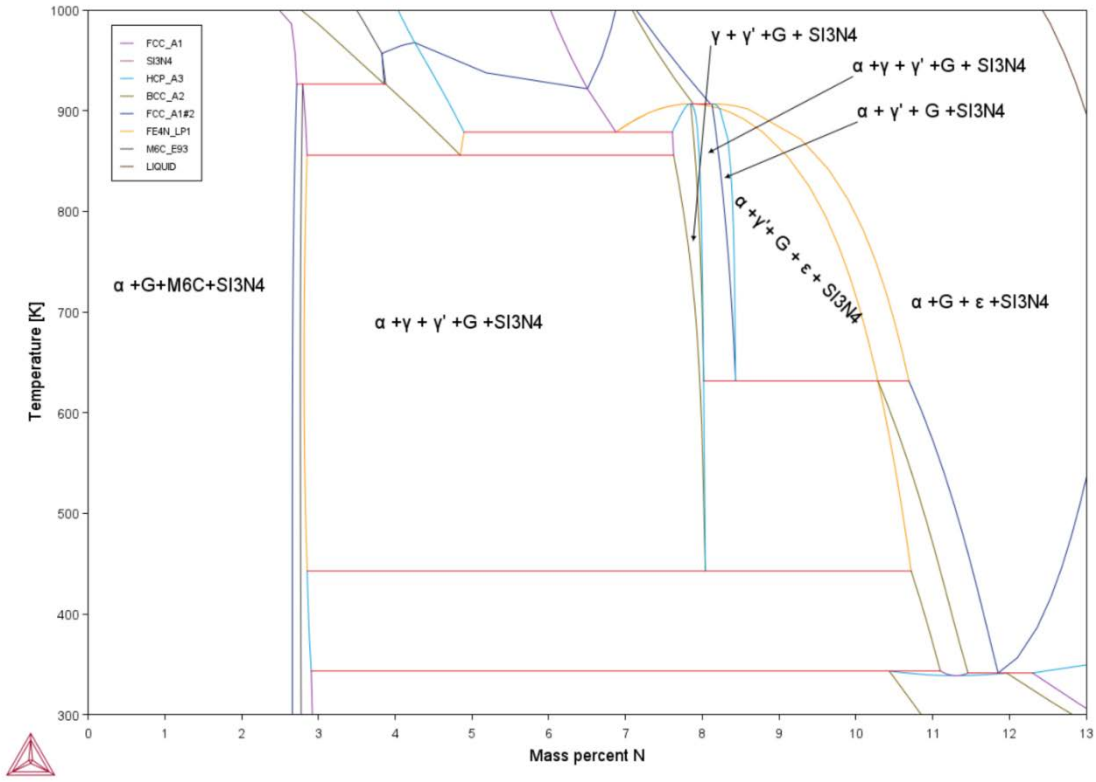

Figure 3.3.1 : Phase Diagram Fe - 3.5 C - 4.0 Si – 1W - N

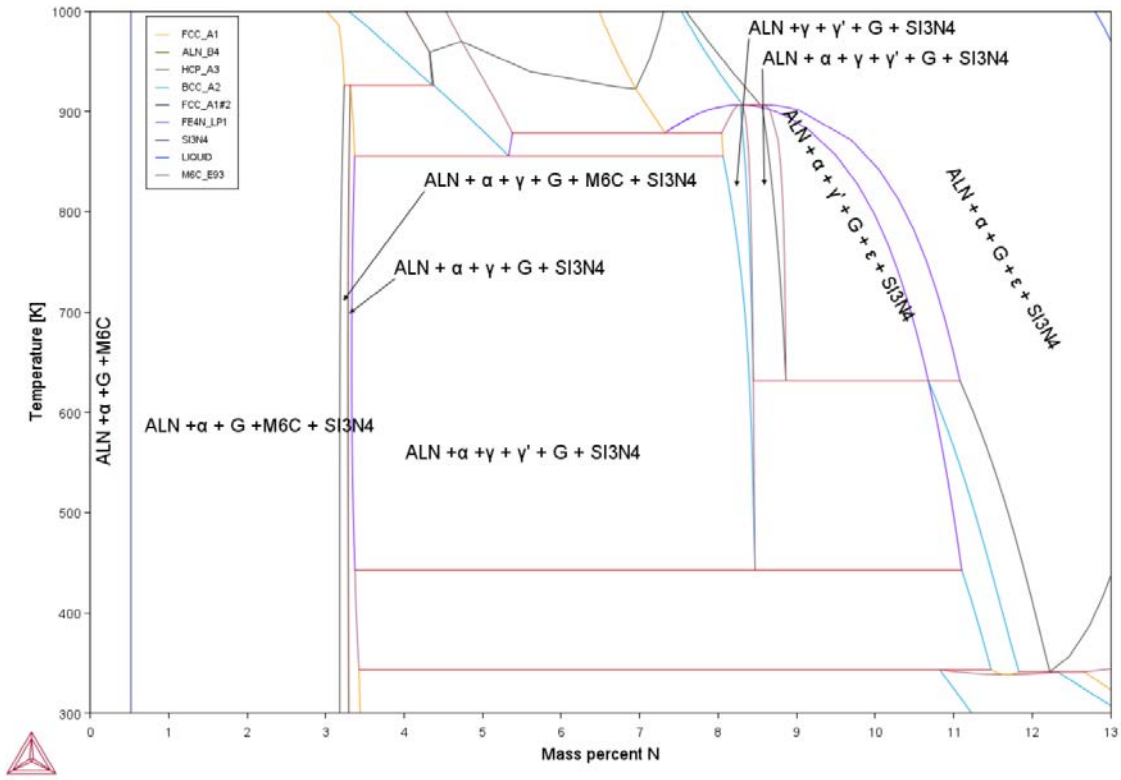

Figure 3.3.2 : Phase Diagram Fe - 3.5 C - 4.0 Si – 1W – 1Al – N

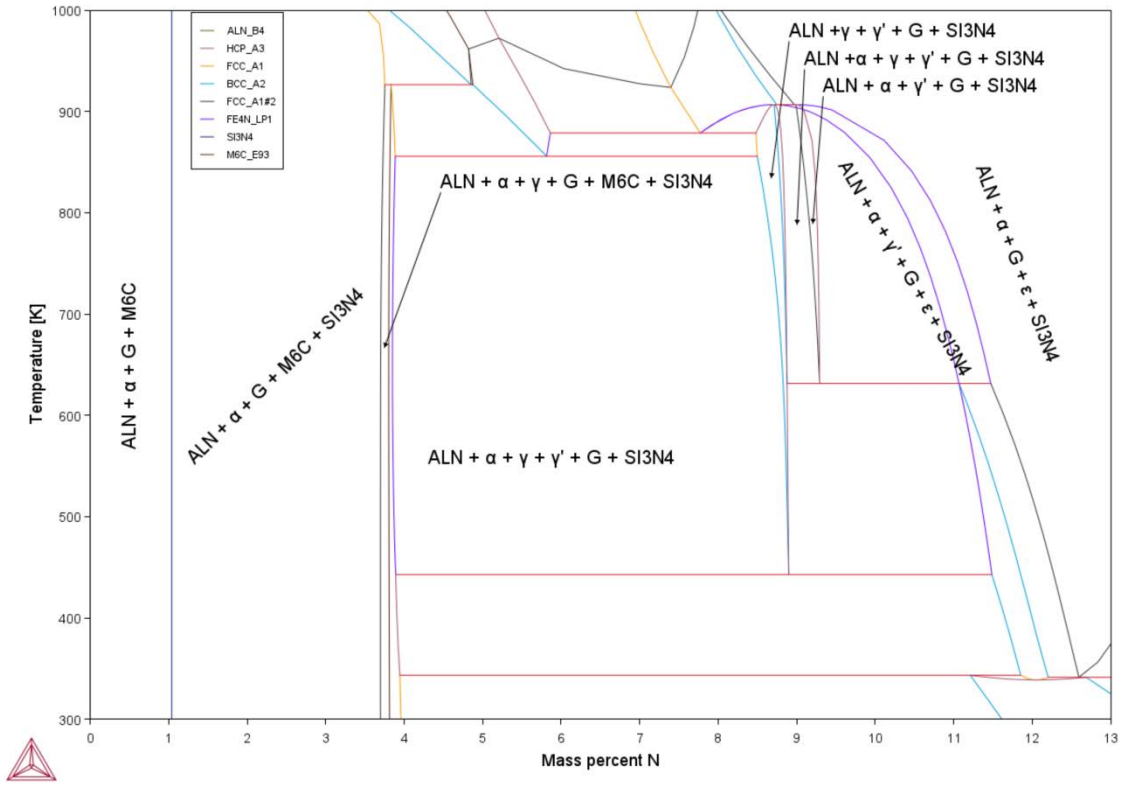

Figure 3.3.3 : Phase Diagram Fe - 3.5 C - 4.0 Si – 1W – 2Al - N

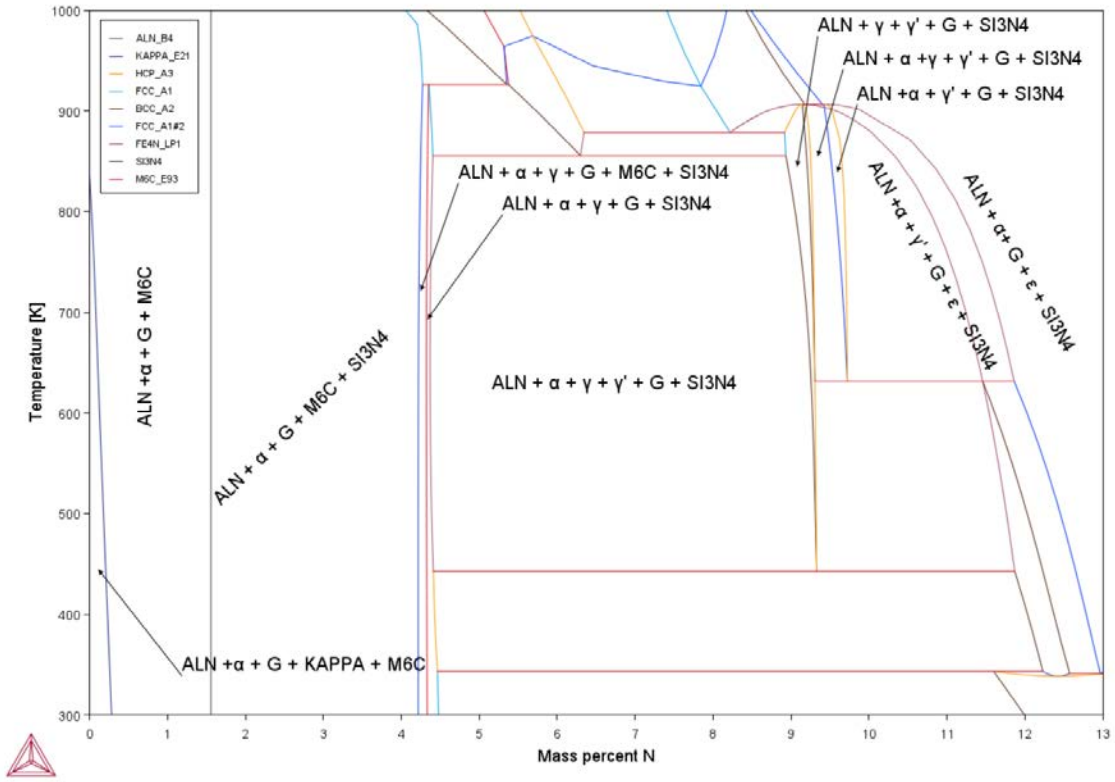

Figure 3.3.4 : Phase Diagram Fe - 3.5 C - 4.0 Si – 1W – 3Al – N

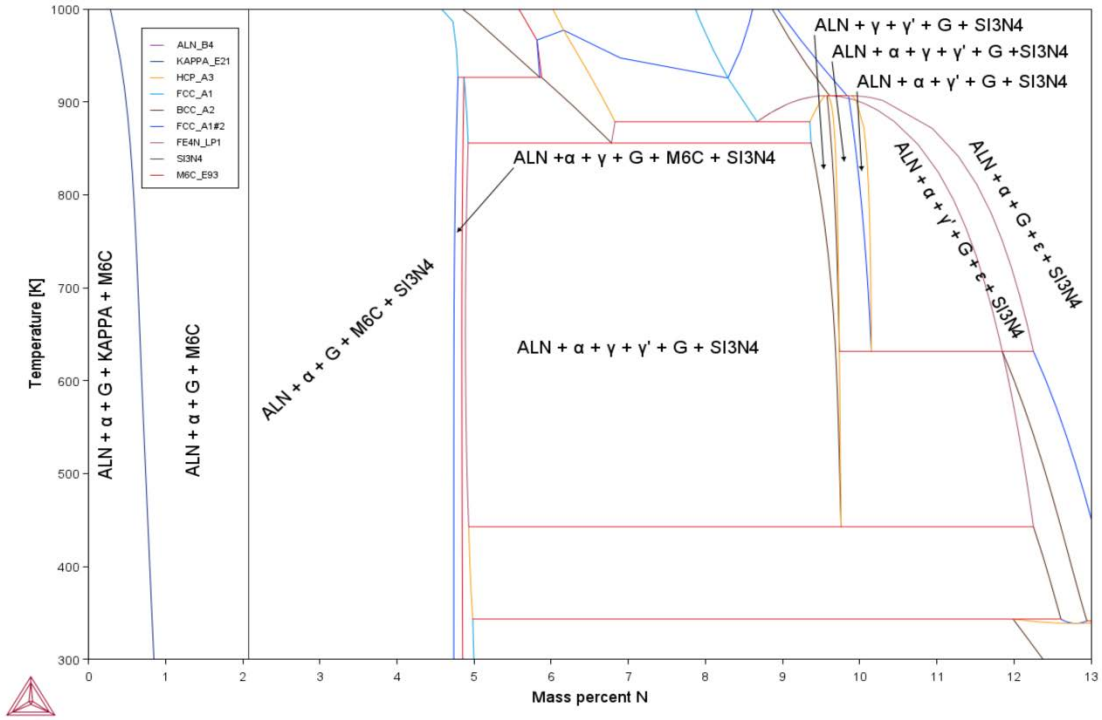

Figure 3.3.5 :Phase Diagram Fe - 3.5 C - 4.0 Si – 1W – 4Al - N

There is a correlation between the distance (x) from the cast iron surface and the weight percentage of N (0-13wt.%), because as we move from the surface (and the distance increases) the N is expected to drop. Thus, phases that appeared in higher N contents will be evident in lower values of distance, near the surface, during and after the nitriding process is complete This is very useful as it is possible to make use of such correlation to model diffusion more accurately. The diffusion can be broken down into two parts: the Compound Layer and the Diffusion Zone. The first consists of three distinct areas of Nitrogen rich phases: ε-nitride, ε+γ'-nitrides, γ'-nitride. The latter consists of a ferritic matrix containing dispersed phases, Graphite, γ, M6C, Si_3N_4 plus AlN and Kappa for depending on the Al content. This two-stage diffusion, resulting from the ε and γ' areas, is a consequence of Nitrogen's low solubility in the phase α, the ferritic matrix of the material under examination. The representation of the Compound Layer and Diffusion Zone is shown on *Figure 3.3.6*.

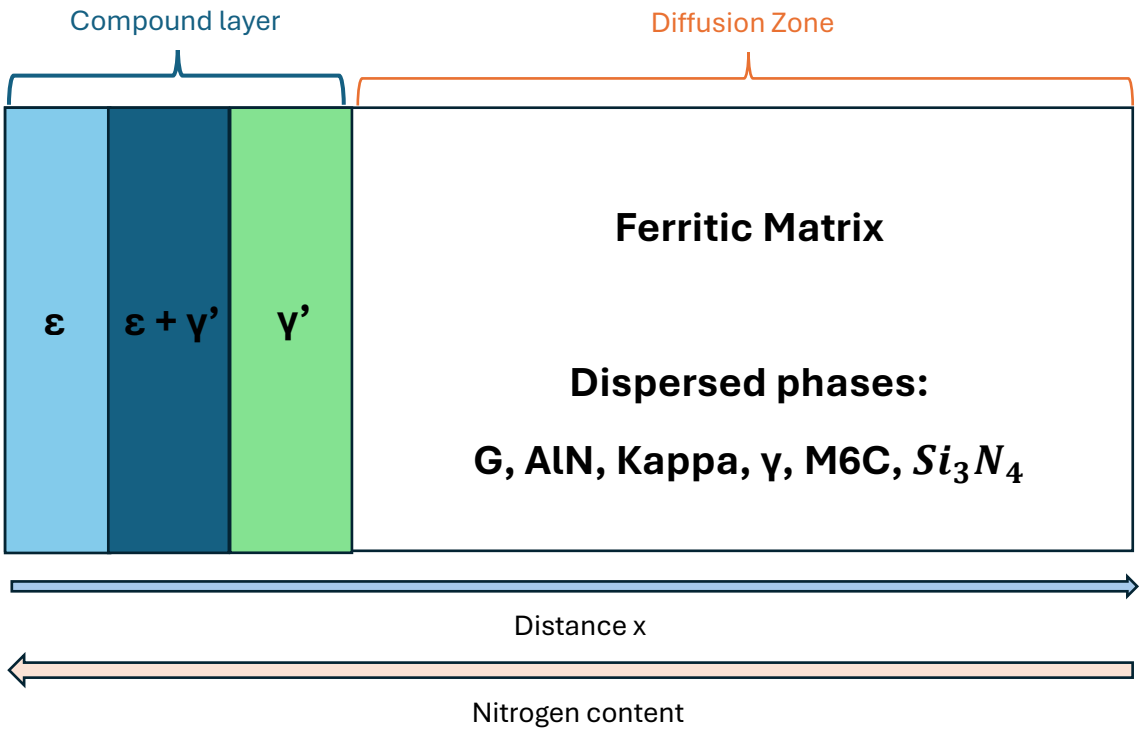

Figure 3.3.6 : Representation of the diffusion zone and compound layer formed during nitriding process.

3.4 Suspension of Si_3N_4

Even if thermodynamics dictate the formation of Si_3N_4 phase, kinetics suggest that this phase will not form. With this knowledge, every calculation involving that phase was temporarily ceased until experimental data confirmed the suspicions. Indeed, as observed by S. Hakan Atapek et al. (2024), there was no formation of this phase at all verifying literature. For this reason, phase diagrams were calculated again without restoring Si_3N_4. Every other thermodynamic

calculation needed to proceed with the diffusion was executed, with Si_3N_4 always being suspended.

First, phase diagrams were recalculated for every Al content, 0%, 1%, 2%, 3% and 4%. It can be easily observed from *Figure 3.4.1* to *Figure 3.4.5* that the suspension of this phase has a major impact on the microstructure of the material in terms of phase composition.

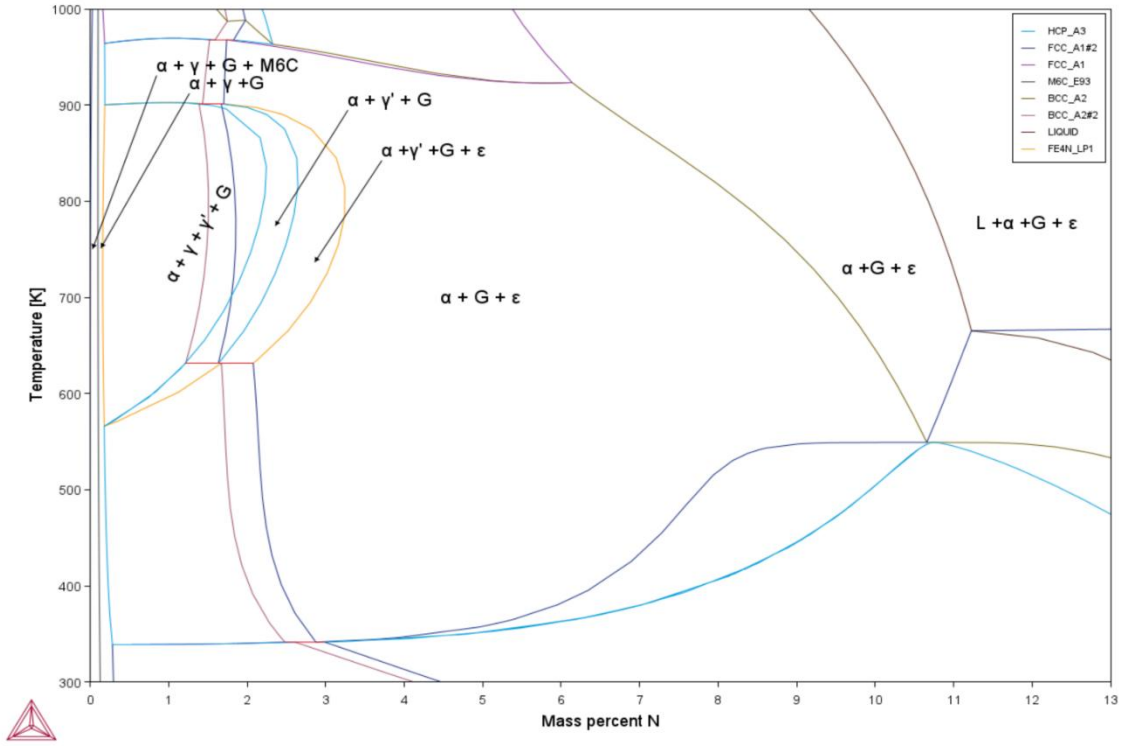

Figure 3.4.1 : Phase Diagram Fe - 3.5 C - 4.0 Si – 1W – N with Si_3N_4 suspended

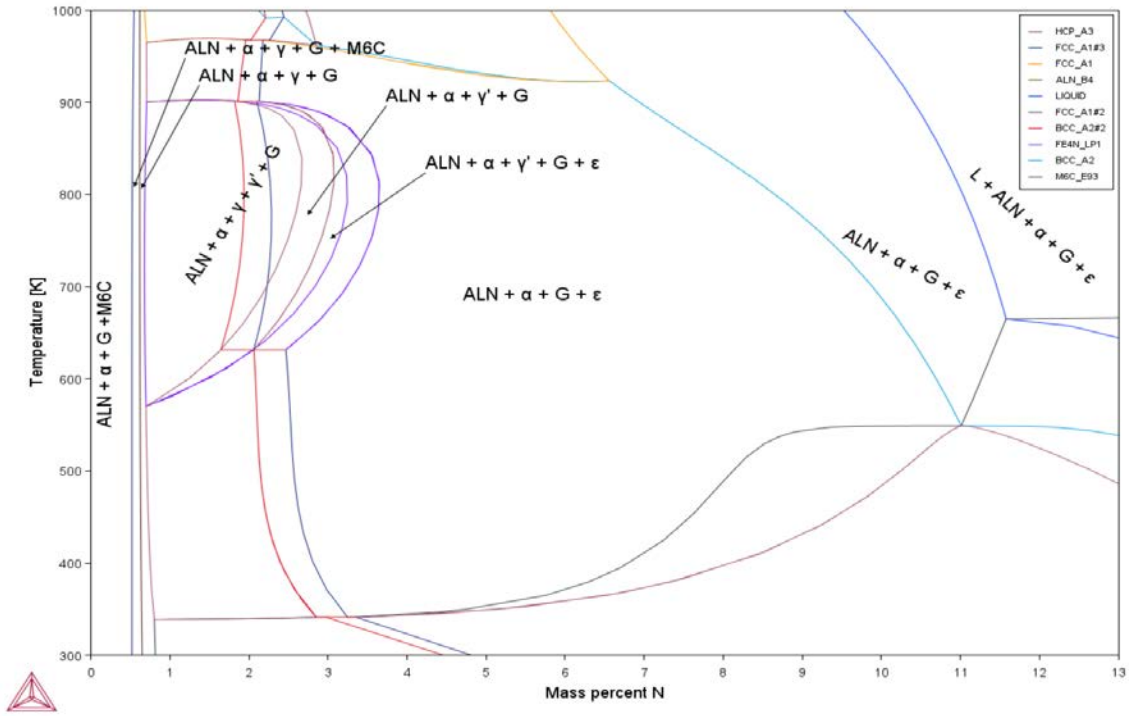

Figure 3.4.2 : Phase Diagram Fe - 3.5 C - 4.0 Si – 1W – 1Al – N with Si_3N_4 suspended.

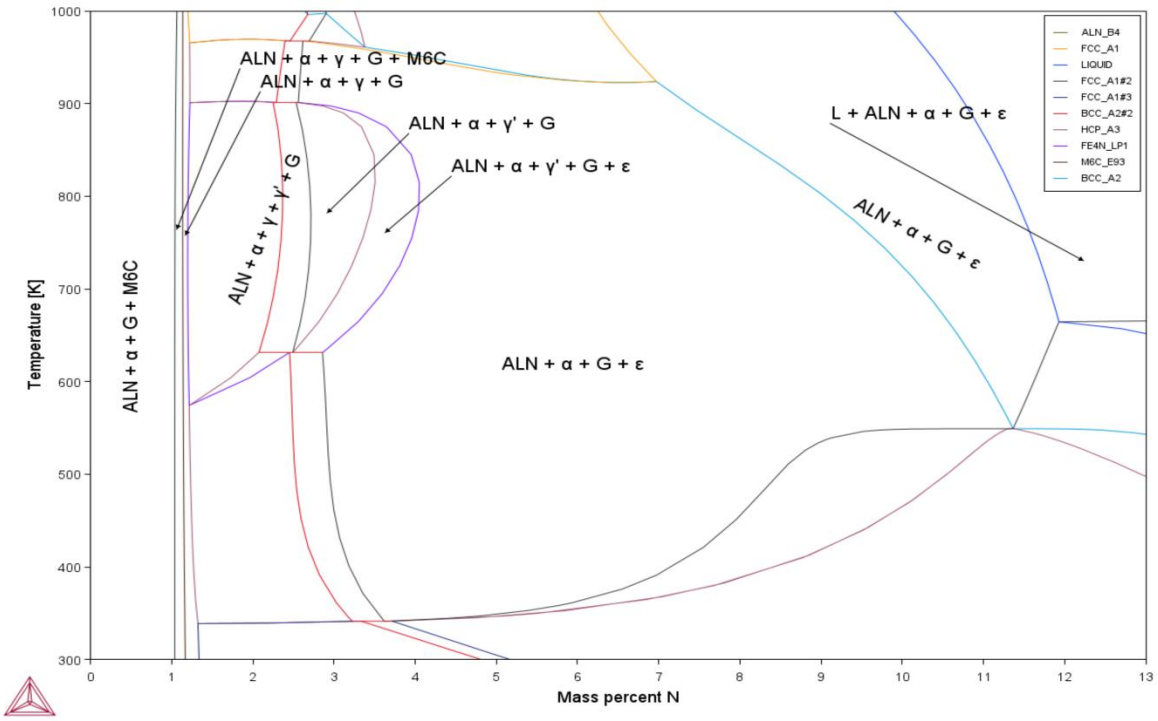

Figure 3.4.3 : Phase Diagram Fe - 3.5 C - 4.0 Si – 1W – 2Al – N with Si_3N_4 suspended.

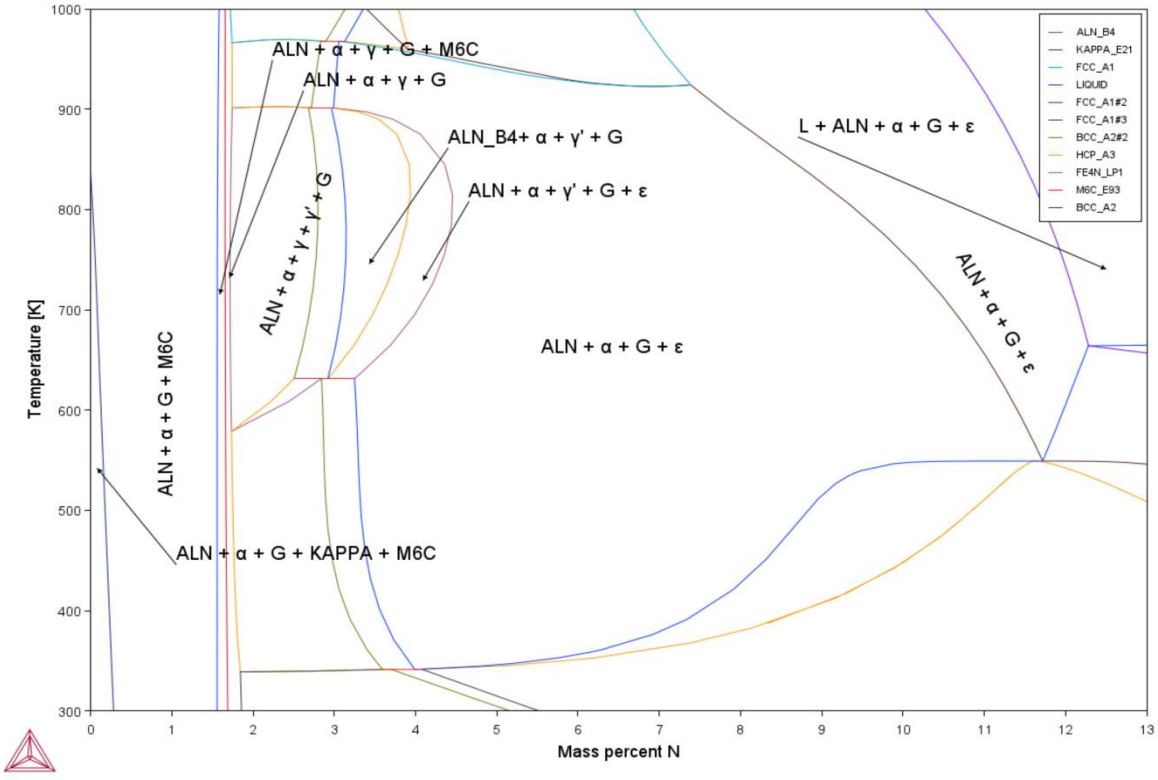

Figure 3.4.4 : Phase Diagram Fe - 3.5 C - 4.0 Si – 1W – 3Al – N with Si_3N_4suspended.

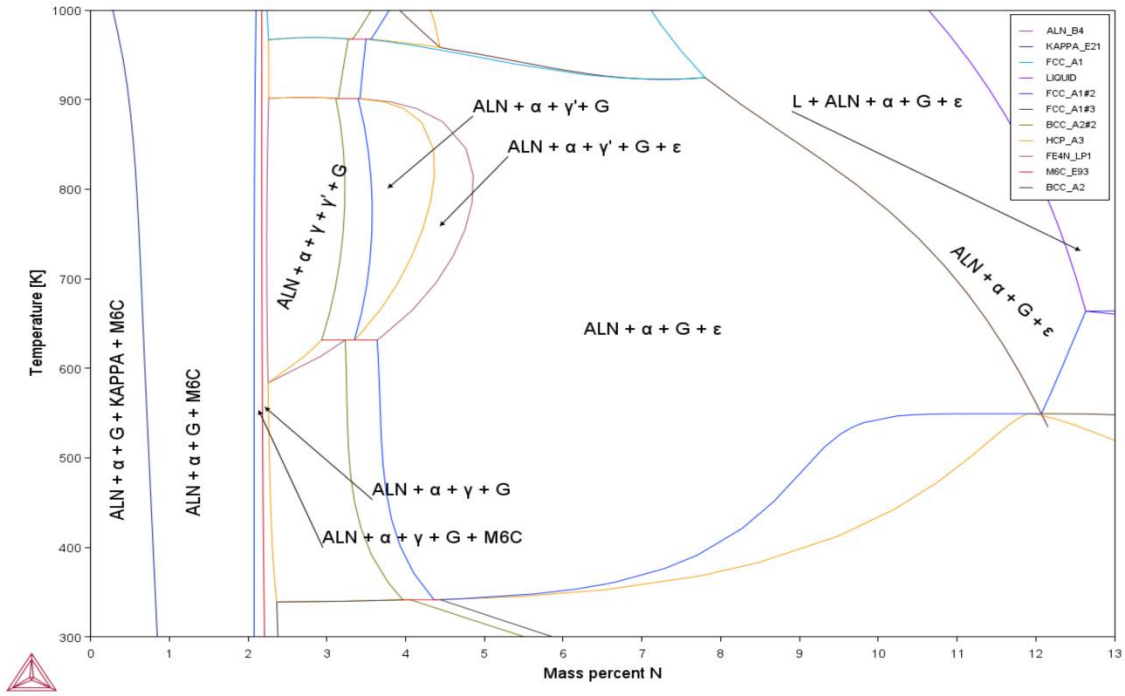

Figure 3.4.5 : Phase Diagram Fe - 3.5 C - 4.0 Si – 1W – 4Al – N with Si_3N_4 suspended.

3.5 Comparison before and after the suspension of Si_3N_4 , for 4 wt.% Al.

To make the impact of the suspension obvious, a side-by-side comparison of the phase diagrams for 4wt.% Al is provided. As a reminder, the two diagrams are the following:

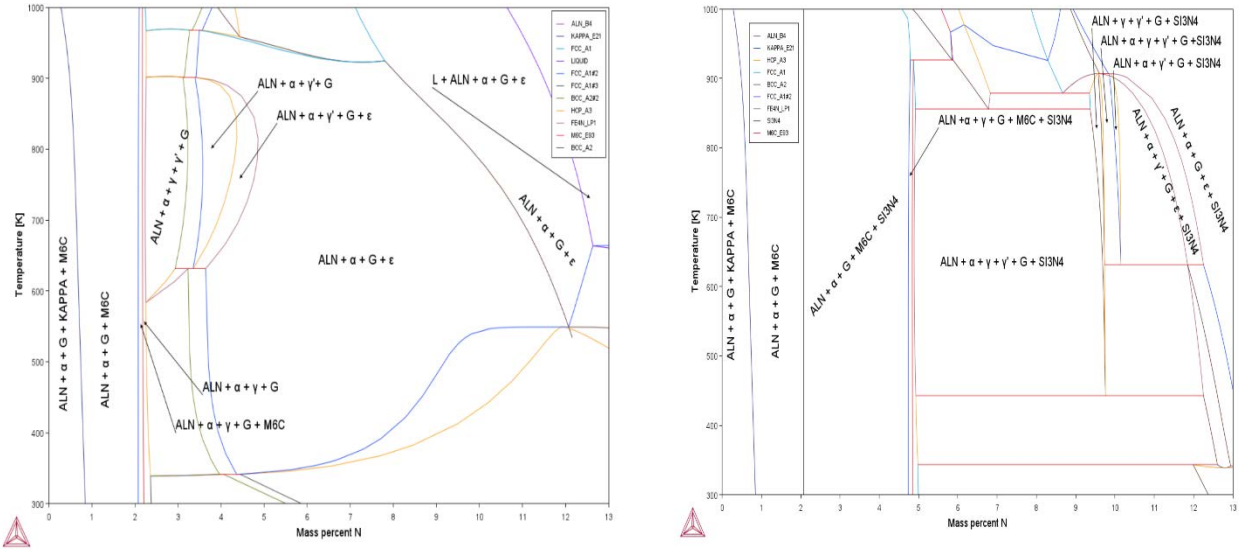

Figure 3.5.1 : Side-by-side comparison before and after the suspension of Si_3N_4 for 4wt. % Al.

When comparing the phase diagrams with suspended and unsuspended phase Si_3N_4 across all five different Al contents, it is evident that the existence of this phase inhibits the

formation of γ' and ε -nitrides in lower N content while pushing the presence of W-rich carbide, M6C, to higher Nitrogen concentration. Without this phase, there is Nitrogen surplus in the ferritic matrix driving the formation of the desired nitrides.

Closer inspection of the phase diagrams unveils interesting things to be spotted. Starting with the impact of Al addition to the cast iron. Every increment to the Al percentage seems to displace the whole diagram to the right, acting as a retardant to creation of ε and γ'. That foreshadows the impact of the Al during the nitriding process which consequently allows more N to diffuse in the matrix and the dispersed phases, given that the creation of the compound layer impedes further penetration of the Nitriding to the inner material.

3.6 Phase Fractions when Si_3N_4 was suspended

Upon phase diagram calculation, it was prudent to calculate how phase fractions changed with varying Nitrogen content at nitriding temperature (510 °C). Some of the points observed in the phase diagrams can appear more intensely in the following figures.

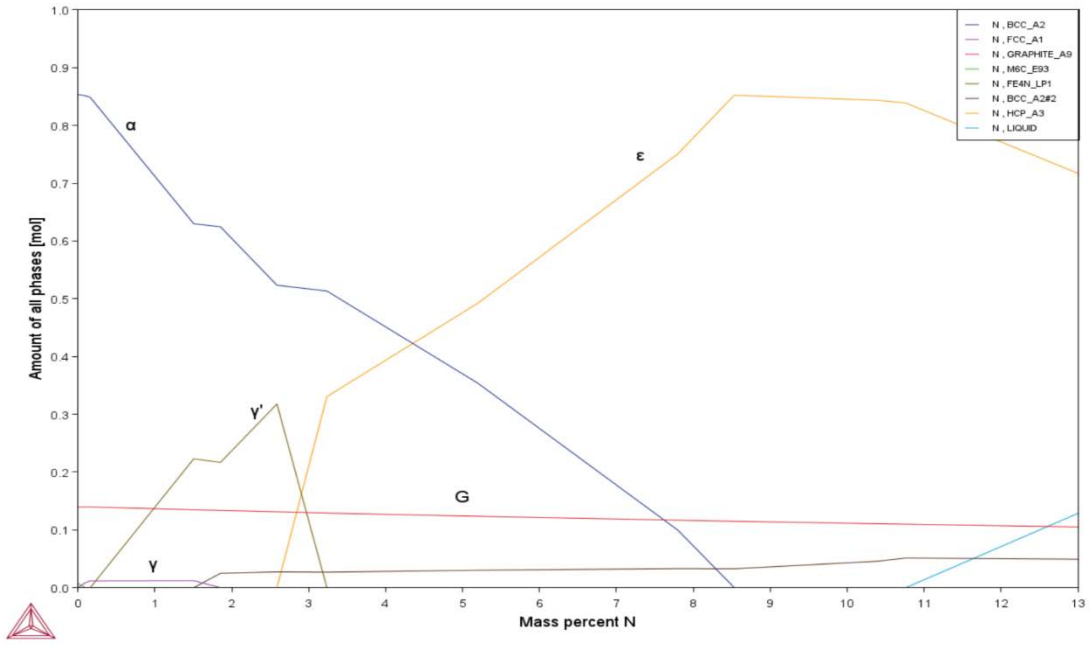

Figure 3.6.1: Phase Fraction Fe - 3.5 C - 4.0 Si – 1W – N at 510 °C with Si_3N_4 suspended.

It must be noted that in the plot above, as well as, in the plots below concerning the Al alloyed materials, there is an unlabeled curve lying in small fractions and expanding for a long Nitrogen content range. This curve truly represents also the ferritic phase but because of software bug, it mistakenly appears as a separate phase. Moreover, the diagonal line appearing in high nitrogen contents (above 10wt.%) is the liquid phase.

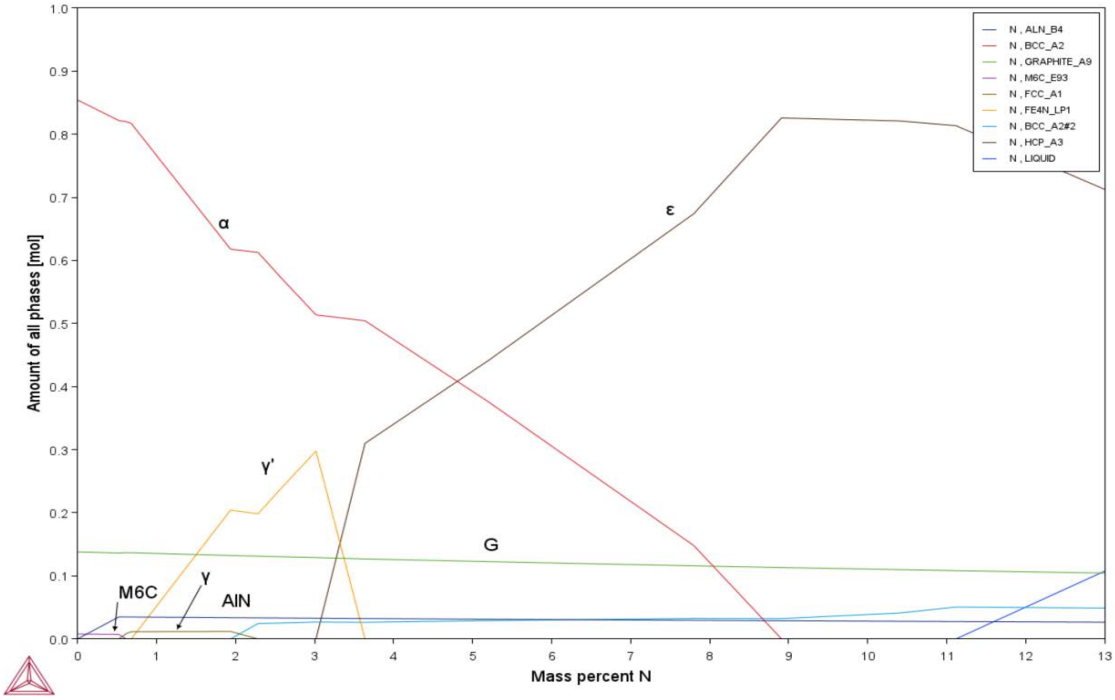

Figure 3.6.2 : Phase Fraction Fe - 3.5 C - 4.0 Si – 1W -1Al – N at 510 °C with Si_3N_4 suspended.

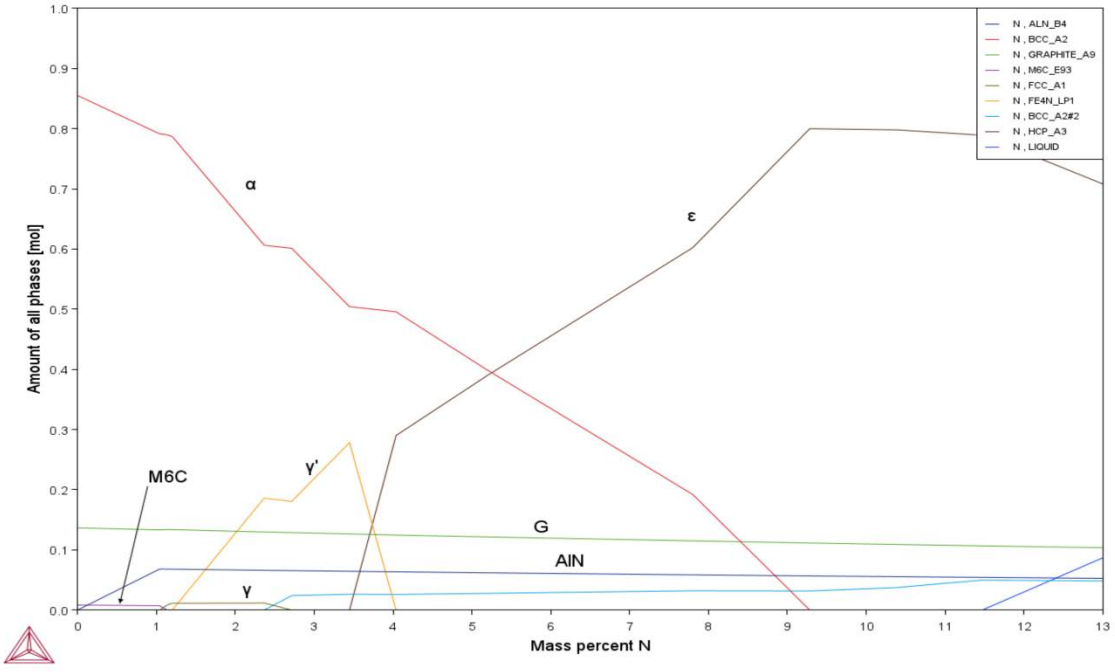

Figure 3.6.3 : Phase Fraction Fe - 3.5 C - 4.0 Si – 1W -2Al – N at 510 °C with Si_3N_4 suspended.

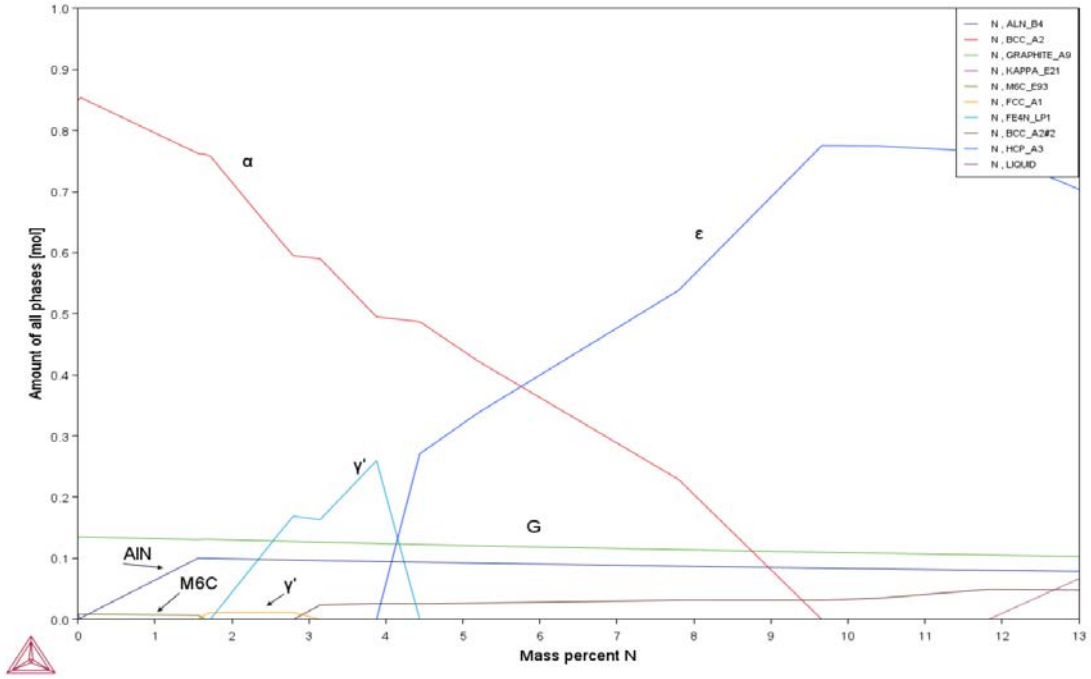

Figure 3.6.4 : Phase Fraction Fe - 3.5 C - 4.0 Si – 1W -3Al – N at 510 °C with Si_3N_4 suspended.

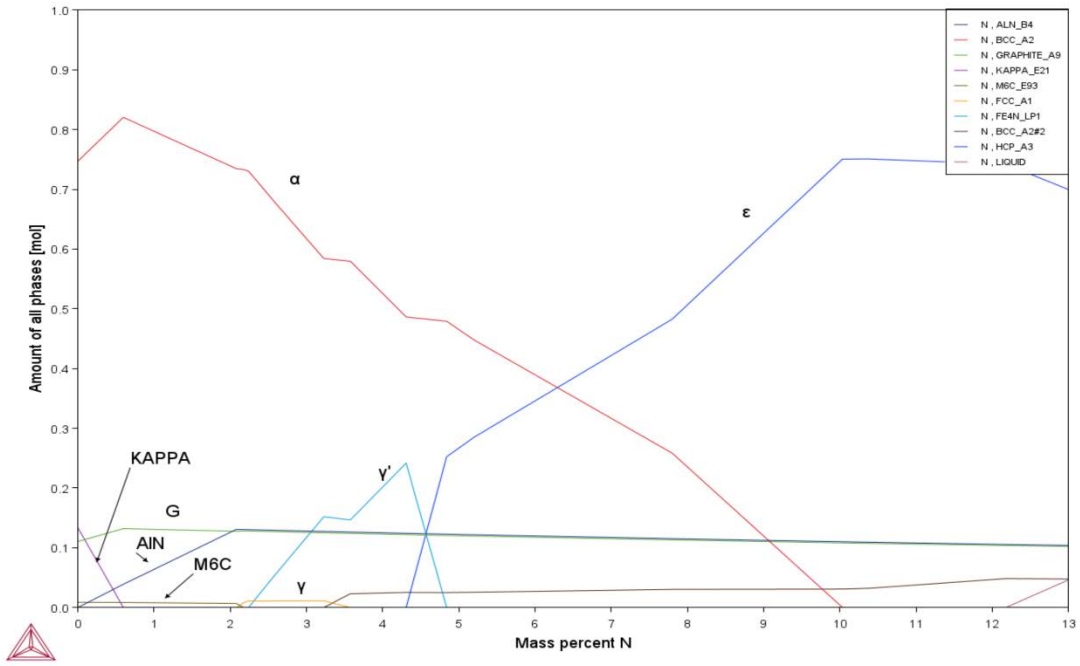

Figure 3.6.5 : Phase Fraction Fe - 3.5 C - 4.0 Si – 1W -4Al – N at 510 °C with Si_3N_4 suspended.

As deduced from the figures, the addition of Al in the base composition has multiple effects in the nitride material. Already observed from phase diagrams, it pushes the γ' and ε nitrides to

higher nitrogen content. Simultaneously, it expands the ferrite field as the α – phase (BCC) Fe-W-N is pushed to higher nitrogen contents, similarly to the nitrides. Also, as expected, the addition of Aluminum increases the maximum almost-constant amount of the AlN phase.

3.7 Useful thermodynamic data for the kinetic simulations

Before proceeding to the kinetics of the nitriding and the diffusion, one last thermodynamic calculation is required. As it will be discussed in more detail in the next chapter, when setting the diffusion simulation, constitution of the ferritic matrix and the dispersed phases with their respective compositions must be also known to use as input arguments. For this reason, a single point equilibrium was calculated for 510 °C and zero nitrogen content, modelling the initial material to undergo nitriding. Again, the tables presented below concern calculations of 0wt%, 1wt%, 2wt%, 3wt% and 4wt% Al.

Ferrite (α)	Volume Fraction	Mass Fraction
	0.883993589	0.950939939
Component	Mole Fraction	Mass Fraction
Fe	0.919984243	0.957995369
Si	0.079974632	0.041880307
W	3.59273E-05	0.00012316
C	5.19742E-06	1.16399E-06
G	Volume Fraction	Mass Fraction
	0.108123922	0.034735336
Component	Mole Fraction	Mass Fraction
C	1	1
Fe	0	0
W	0	0
Si	0	0
M6C	Volume Fraction	Mass Fraction
	0.007882489	0.014324725
Component	Mole Fraction	Mass Fraction
W	0.349966834	0.689917747
Fe	0.466761337	0.279512683
C	0.142857143	0.018398733
Si	0.040414686	0.012170837

Table 3.7.1 : Composition of each phase Fe – 3.5C – 4Si – 1W at 510°C

Ferrite (α)	Volume Fraction	Mass Fraction
	0.880008017	0.943096602
Component	Mole Fraction	Mass Fraction
Fe	0.864461841	0.928041584
Si	0.076261234	0.041171815
Al	0.059259844	0.030736641
W	1.39305E-05	4.92326E-05
C	3.15027E-06	7.2736E-07
G	Volume Fraction	Mass Fraction
	0.102754789	0.034298009
Component	Mole Fraction	Mass Fraction
C	1	1
Fe	0	0
Al	0	0
W	0	0
Si	0	0
M6C	Volume Fraction	Mass Fraction
	0.008124724	0.014500816
Component	Mole Fraction	Mass Fraction
W	0.33346252	0.683052547
Fe	0.433112221	0.269490673
Si	0.090568115	0.028339567
C	0.142857143	0.019117213
Al	0	0

Ferrite (α)	Volume Fraction	Mass Fraction
	0.774545838	0.835016881
Component	Mole Fraction	Mass Fraction
Fe	0.859107916	0.924869744
Si	0.085620918	0.04635401
Al	0.055258896	0.028741494
W	9.63354E-06	3.41415E-05
C	2.63706E-06	6.10566E-07
G	Volume Fraction	Mass Fraction
	0.085108755	0.028598177
Component	Mole Fraction	Mass Fraction
C	1	1
Fe	0	0
Al	0	0
W	0	0
Si	0	0
M6C	Volume Fraction	Mass Fraction
	0.008600135	0.014784052
Component	Mole Fraction	Mass Fraction
W	0.308221775	0.671620364
Fe	0.380881928	0.252108286
Si	0.168039154	0.055934765
C	0.142857143	0.020336585
Al	0	0

Table 3.7.2 : Composition of each phase Fe – 3.5C – 4Si – 1W – 1Al at 510°C (left) and Composition of each phase Fe – 3.5C – 4Si – 1W – 2Al at 510°C (right).

Ferrite (α)	Volume Fraction	Mass Fraction
	0.880008017	0.943096602
Component	Mole Fraction	Mass Fraction
Fe	0.864461841	0.928041584
Si	0.076261234	0.041171815
Al	0.059259844	0.030736641
W	1.39305E-05	4.92326E-05
C	3.15027E-06	7.2736E-07
G	Volume Fraction	Mass Fraction
	0.102754789	0.034298009
Component	Mole Fraction	Mass Fraction
C	1	1
Fe	0	0
Al	0	0
W	0	0
Si	0	0
KAPPA	Volume Fraction	Mass Fraction
	0.008371737	0.007683289
Component	Mole Fraction	Mass Fraction
Fe	0.618096566	0.818168303
Al	0.206032189	0.131763671
C	0.175871245	0.050068027
W	0	0
Si	0	0
M6C	Volume Fraction	Mass Fraction
	0.008865457	0.014922101
Component	Mole Fraction	Mass Fraction
W	0.293400524	0.66703537
Fe	0.337783956	0.233272321
Si	0.225958377	0.078474258
C	0.142857143	0.02121805
Al	0	0

Ferrite (α)	Volume Fraction	Mass Fraction
	0.774545838	0.835016881
Component	Mole Fraction	Mass Fraction
Fe	0.859107916	0.924869744
Si	0.085620918	0.04635401
Al	0.055258896	0.028741494
W	9.63354E-06	3.41415E-05
C	2.63706E-06	6.10566E-07
G	Volume Fraction	Mass Fraction
	0.085108755	0.028598177
Component	Mole Fraction	Mass Fraction
C	1	1
Fe	0	0
Al	0	0
W	0	0
Si	0	0
KAPPA	Volume Fraction	Mass Fraction
	0.131433302	0.121432312
Component	Mole Fraction	Mass Fraction
Fe	0.618096566	0.818168303
Al	0.206032189	0.131763671
C	0.175871245	0.050068027
W	0	0
Si	0	0
M6C	Volume Fraction	Mass Fraction
	0.008912105	0.01495263
Component	Mole Fraction	Mass Fraction
W	0.289522228	0.66687209
Fe	0.321743875	0.225116398
Si	0.245876754	0.086514499
C	0.142857143	0.021497013
Al	0	0

Table 3.7.3 : Composition of each phase: Fe – 3.5C – 4Si – 1W – 3Al at 510°C (left) Fe – 3.5C – 4Si – 1W – 4Al at 510°C (right).

Chapter 4 : Nitriding – Kinetic Simulations

4.1 DICTRA – Simulation Tool

After obtaining equilibrium data from Thermocalc software, it is possible to proceed to the kinetic calculation to examine the nitriding process. Finding the exact phase composition and profiles of the alloying elements involves solving differential equations, as explained extensively in the next section. However, in most cases such differential equations are insoluble and solution is approached through numerical methods. Thus, the DICTRA module, part of Thermocalc software, is implied to make the necessary computations. Diffusion Controlled TRAnsformations (DICTRA) is used in multicomponent alloys to simulate complex systems using data for multicomponent thermodynamics and diffusion.[23][24] It is a widely used software in research and development of materials, giving useful information about microstructure without the necessity of real experiments. Apart from time and cost efficiency, it provides a way to have estimation on microstructures in conditions that cannot be reproduced in an experiment for limiting factors like long-term analysis, e.g. coarsening of carbides in a steel pipe after 20 years of operation. Therefore, DICTRA module as a computational tool is used as a guide to more targeted experiments and as a replacement to analytical solutions.

4.2 Analytic Solution

As mentioned above, the nitriding process can be described by a set of differential equations and the resulting microstructure and composition is the solution to this set. It is a heat-treatment process and consequently the dominant kinetic mechanism undergoing is the diffusion of nitrogen atoms in interstitial positions located inside the ferritic matrix of the alloy. Nitrogen profile in the matrix as time advances can be estimated using Fick's 2nd Law of Diffusion. Assuming constitution-independent diffusion coefficient, constant surface concentration and uniform concentration across the material the concentration profile c(x,t) can be calculated from the following differential equation:

$$\frac{\partial c}{\partial t} = D\frac{\partial^2 c}{\partial x^2} \qquad \{4a\}$$

with initial condition: $c(x,0) = 0$ {4b}

and boundary conditions: $c(0,t) = C_s$ {4c}

$c(\infty,t) = 0$ {4d}

Therefore, the concentration profile can be determined as [12]:

$$C(x,t) = A + Berf\left(\frac{x}{2\sqrt{Dt}}\right) \qquad \{4e\}$$

Nevertheless, these assumptions can lead to inaccurate results and provide insufficient information about the resulting microstructure, as there is no other information available than the concentration profile and thus, phase composition and ferritic matrix constitution remain unknown.

4.3 Model for Cast Iron Nitriding

To obtain more information about the resulting microstructure and better understand the impact of various parameters in the nitriding process it was necessary to make use of the DICTRA software. It is obvious that the more realistic inputs inserted, the more accurate the simulation results will be. However, trading accuracy with computational cost and minimizing the probability of an error occurring is a common practice to simplify the model used for the simulation. The model used is explicitly presented in the paragraphs to follow.

A model depicting almost accurately the entire process could be a relatively large cell so the material can be considered as semi-infinite containing grain boundaries. The shape of the cell that can be rectangular, spherical or cylindrical is chosen to be rectangular as the diffusion examined concerns a closed system with just a boundary condition of Nitrogen concentration. To continue with, there should be 3 inactive regions on the nitriding bound. The first region should contain only the ε phase, the second region ε and γ' phases and the last one only the γ' phase. These 3 regions must be attached to an active region of ferritic matrix with G and M_6C as dispersed phases containing also AlN and Kappa phases if the cast iron contains aluminum. *Figure 3.3.6* illustrates the model described above if the compound layer regions are chosen to be inactive and in the left bound of the cell constant nitrogen concentration is assumed as in *Figure 3.4.1*.

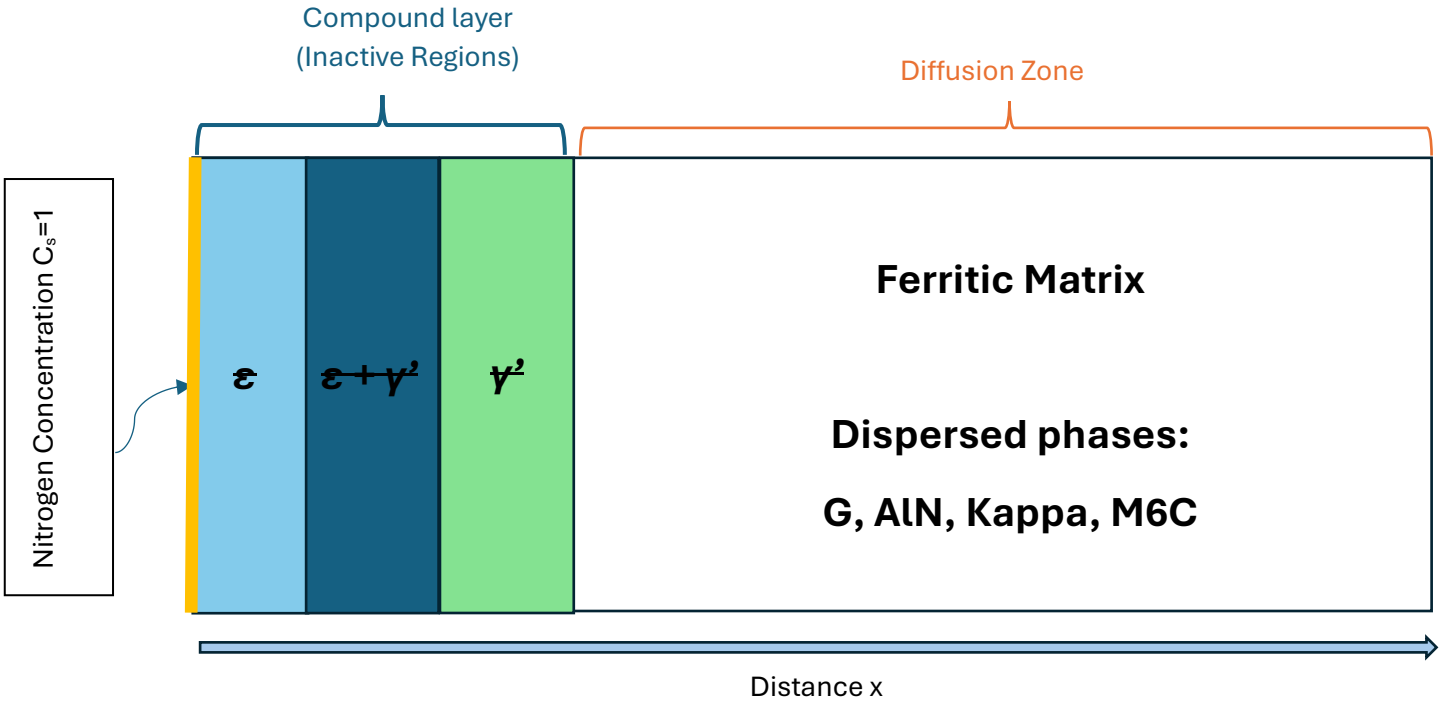

Figure 4.3.1 : Representation of a realistic model for the nitriding process.

However, simplifications had to be made because of software's incapabilities. Existence of compound layer and ε, γ' phases as matrix phases impedes deeper diffusion of Nitrogen in the cell. Consequently, these phases must be integrated, as spherical dispersed phases, into the diffusion zone region that will be the only region of the cell hereafter. Cell size also had to be adjusted as finite but estimated not to affect the diffusion.

After the assumptions made, the resulting model used for the simulations has the form described hereupon. The composition of the cast iron to be nitride is Fe-3.5wt%C–4%Si–1%W-xAl where for aluminum content values of 0, 1, 2, 3 and 4% were chosen. As further explained later on this thesis there is a focus on high aluminum alloying as it boosts the nitriding process. Concerning the cell geometry, a rectangular geometry was set with width of 3mm as nitriding depth is expected not to surpass 200-300μm in the defined simulation time. When inserting the phases of the model, once again the Si_3N_4 phase was suspended and no kinetic simulations were executed taking into account this phase. As a result, the model cell used had only one region with ferritic matrix and inside there were the rest of the phases dispersed. Analytically, the phases dispersed into the ferritic matrix where G, ε, γ' and M_6C for no aluminum content, AlN was added when simulating 1% and 2%, and when simulating 3% and 4% Al Kappa phase is also added as thermodynamics suggest. Phases with nitrogen instead of being set as inactive, were set as active but with zero composition, while the rest of the phases' compositions were entered based on the equilibrium values presented in the *Table 3.7.1* through *Table 3.7.3*. As far as the global conditions are concerned, pressure was set to 1bar (10^5 Pa) with a temperature of 783K (~510°C) while the setting gas as the reference state for the nitrogen. The lower boundary of the system was characterized as mixed with zero flux for all elements apart from Nitrogen that activity was set at 500 (Act(N)=500). Finally, the simulation time was set to 144,000 seconds (40 hours) and a time step of 500 seconds while plots concerned time of 43,200 seconds (12 hours) and 144,000 seconds (40 hours).

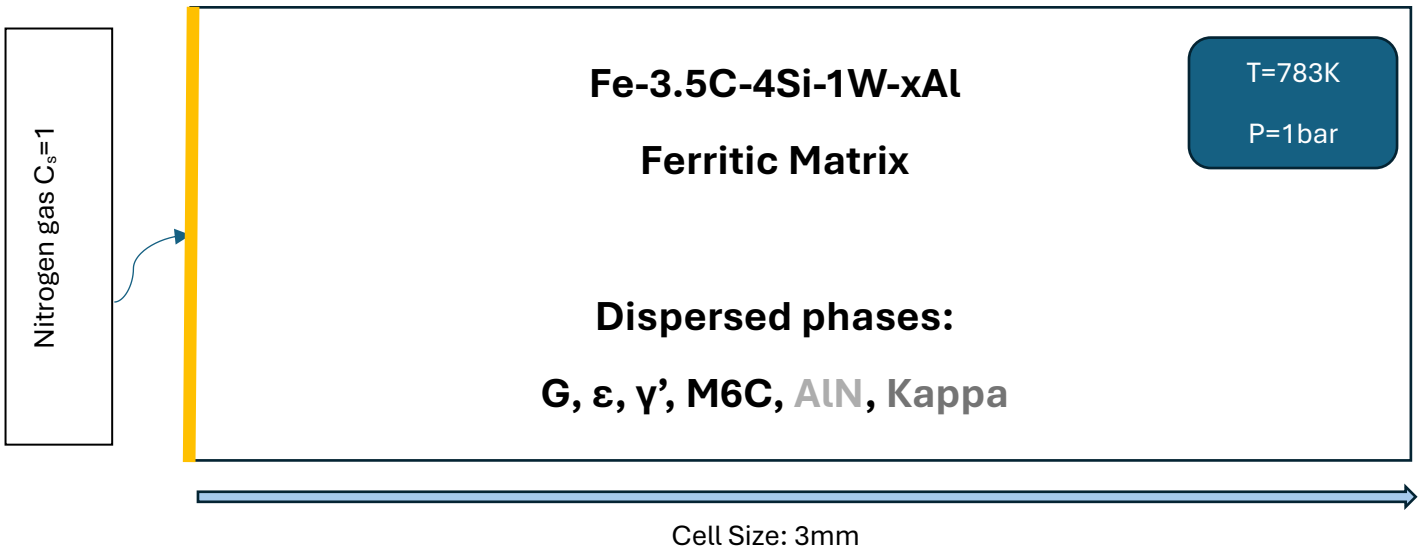

Figure 4.3.2 :Representation of the model used for the nitriding process.

4.4 Nitriding Simulation of Base Alloy

Simulation of the alloy without aluminum (Fe-3.5wt%C–4%Si–1%W) is the first step to study the effects of varying different parameters. In the figures to follow there is a clear view of the nitriding effects. For a better understanding of the figures, it must be noted that the bold curves concern time of 40 hours, whereas the light curves, time of 12 hours. Moreover, the nitrogen profiles in each phase at the end of the process were plotted with the help of Matlab software. Also, in these plots, nitrogen percentage in γ' and ε is indicated even in depth where these phases are not present, but it comes up as a computational error and should not be considered. A vertical line is drawn at the point where ε phase ceases to exist to facilitate locating this point.

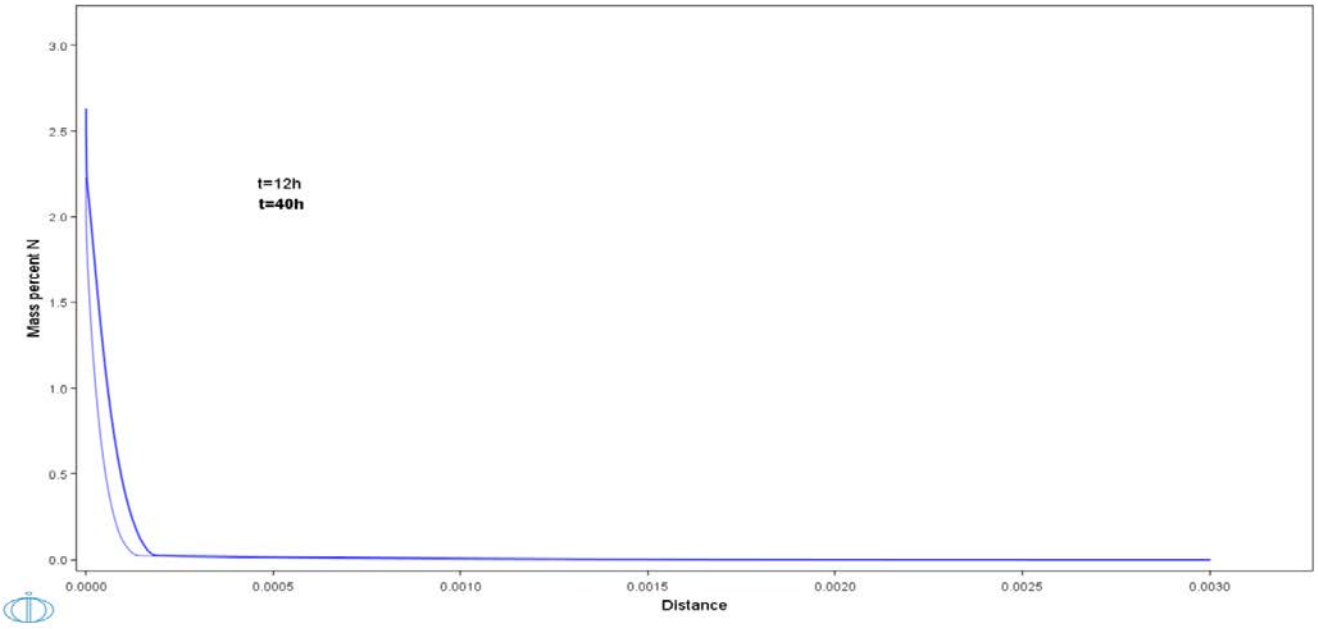

Figure 4.4.1 : Distance from surface vs Weight percent of nitrogen after 12 and 40 hours for 0% Al.

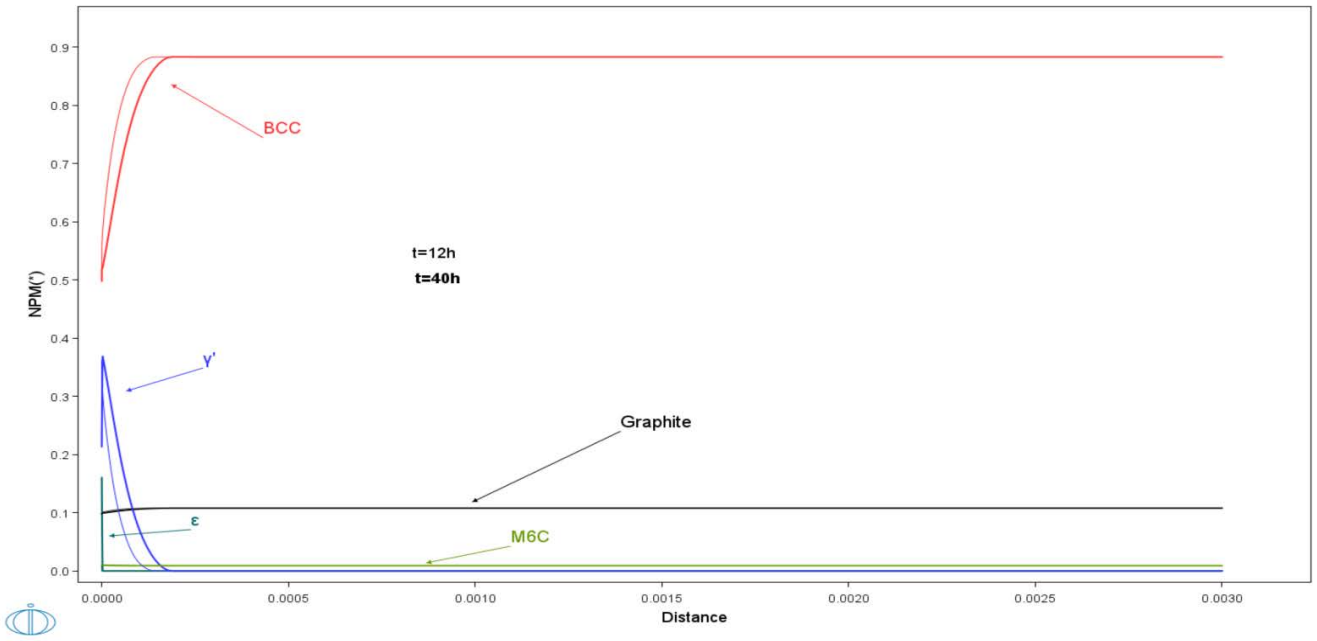

Figure 4.4.2 : Distance from surface vs Phase Fraction of all phases after 12 and 40 hours for 0% Al.

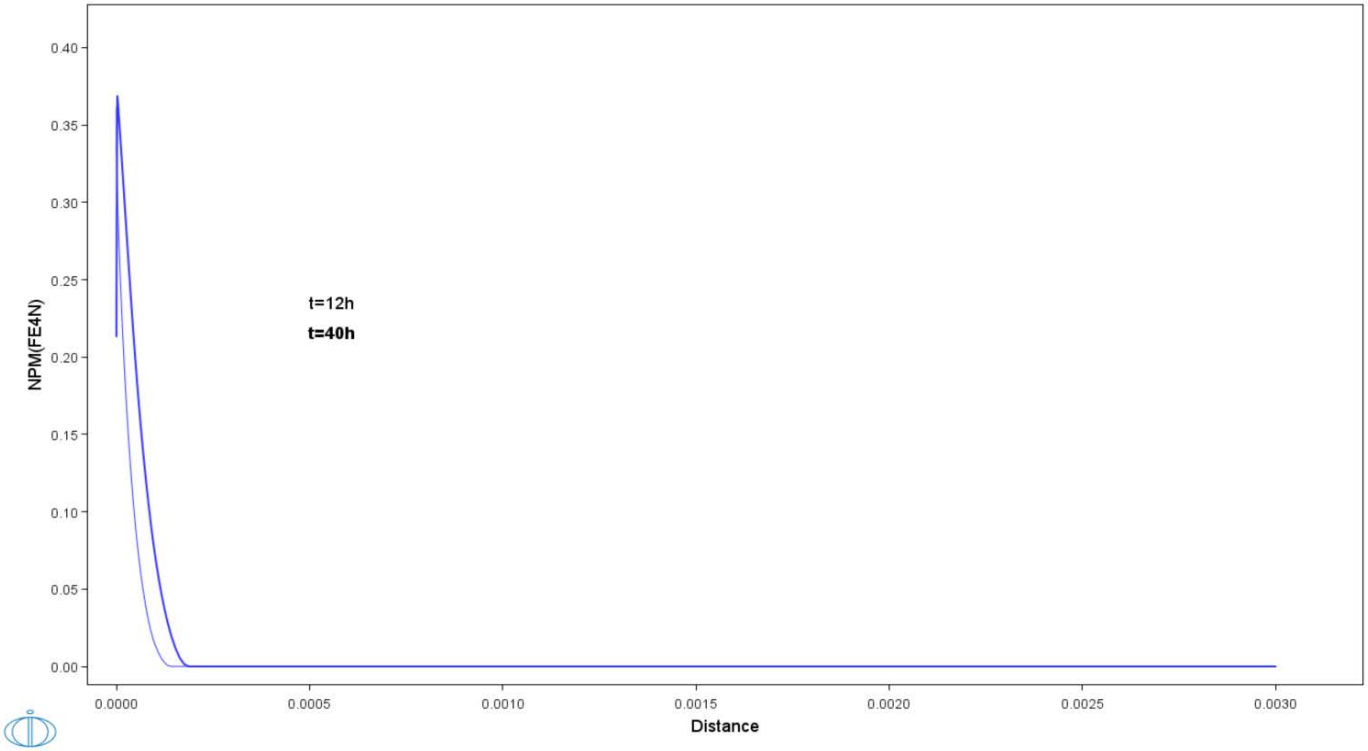

Figure 4.4.3 : Distance from surface vs Phase Fraction of γ' phase after 12 and 40 hours for 0% Al.

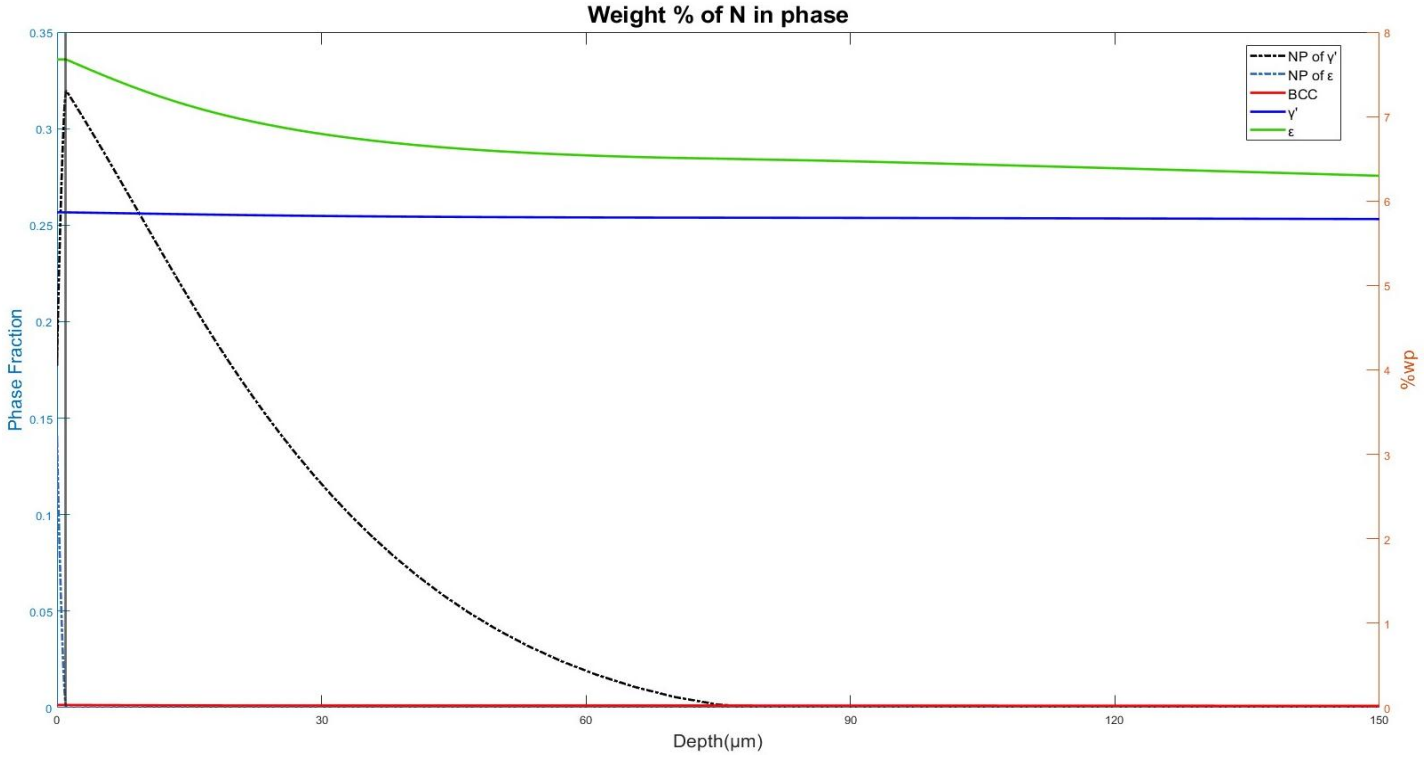

Figure 4.4.4 : Distance from surface vs nitrogen weight percent in phases and Phase Fraction of γ' and ε phases after 40 hours for 0% Al.

At nitriding time of 12 hours nitrogen is absorbed from the material, reaching at distance 40 μm forming only γ' because 2.2%w nitrogen is not sufficient to form ε. Phase fraction of γ' peaks at 0.27 and reduces to zero along with the nitrogen weight percent. At nitriding time of 40 hours, effectiveness of the nitriding reaches a depth of 75 μm with a maximum of Nitrogen content (~2.7%wp) near the surface. As can be extracted from the plots, phase distribution follows the forecast as well as the experimental data. A thin layer of several μm of ε phase is formed on the surface. Moving deeper into the material γ' phase starts to grow against ε phase in approximately 10 μm that these phases coexist reaching its peak fraction of 33% at distance where the ε phase has completely disappeared then reducing to zero gradually deep to 75 μm. From *Figure 4.4.4* it is evident that the nitrogen profile in each phase at the end of the process is practically constant and that α phase can absorb only a tiny amount of nitrogen leading to the presence of nitrogen in the material equivalent to ε or γ' phase formation.

The rest of the dispersed phases seem to be slightly affected by the process. Graphite phase fraction slightly reduces in the presence of nitrogen drafting away from the 13.9% of the starting composition down to 10.5% at the surface of the material containing more nitrogen. M_6C phase is practically unaffected by the process. Thus, as evident from *Figure 4.4.2* ε nitride and γ' both grow against α phase which varies largely to account for the phase constitution balance.

4.5 Effect of Aluminum Addition

The next step was simulating the alloy also for aluminum content of 1, 2,3 and 4% with the rest of the alloying elements always invariable and iron balanced. As expected from the thermodynamic calculations which indicated that increasing aluminum boost nitriding, DICTRA simulations confirmed the assumptions. The following figures concerning the 1 and 2% aluminum content, again, show nitrogen content and phase fraction of phases as a function of distance. Similarly, the light curves account for nitriding time of 12 hours and the bold for time of 40 hours.

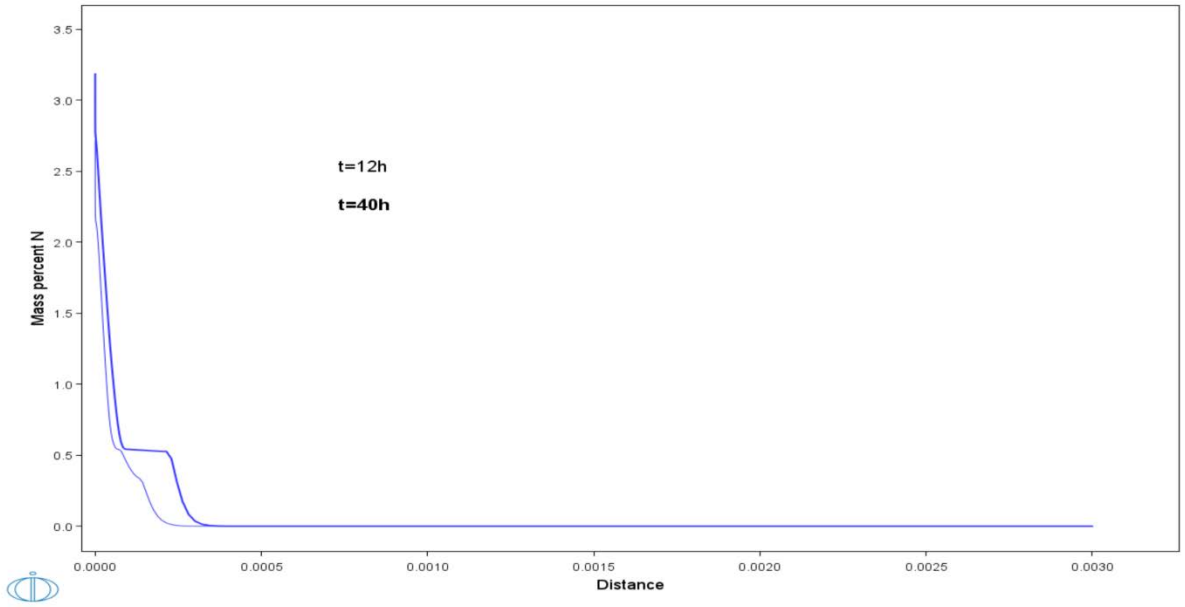

Figure 4.5.1 : Distance from surface vs Weight percent of nitrogen after 12 and 40 hours for 1% Al.

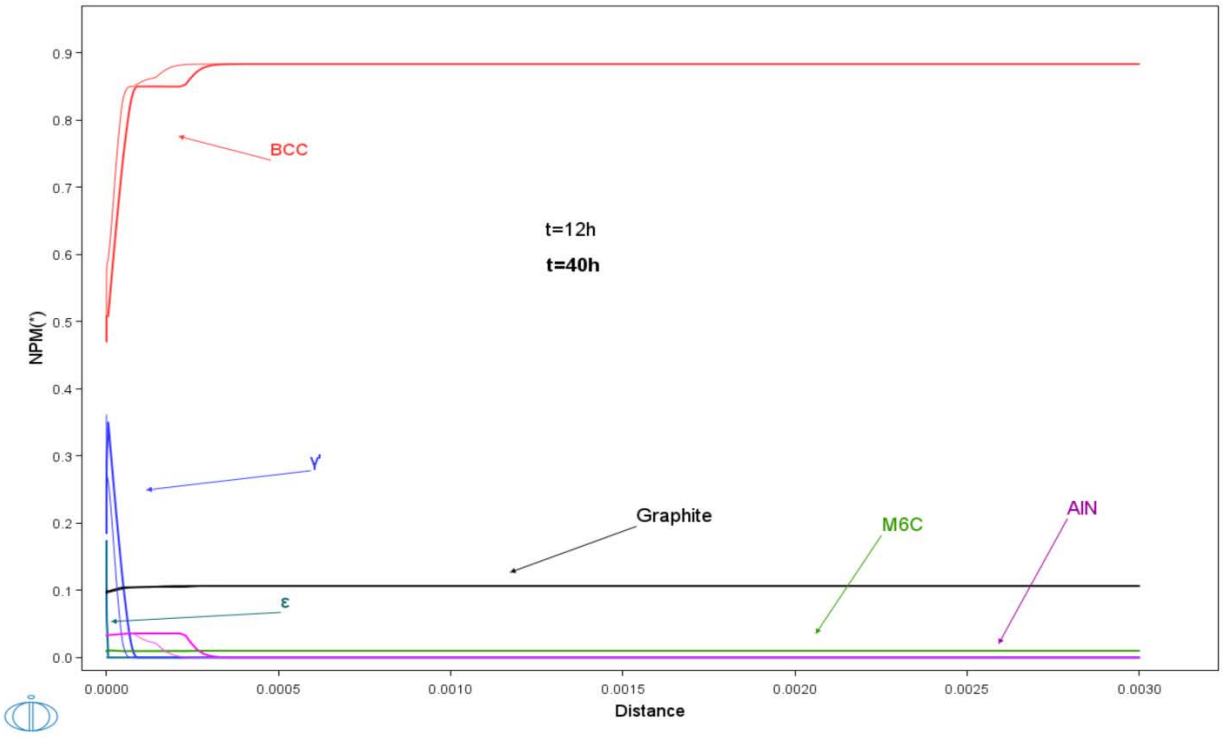

Figure 4.5.2 : Distance from surface vs Phase Fraction of all phases after 12 and 40 hours for 1% Al.

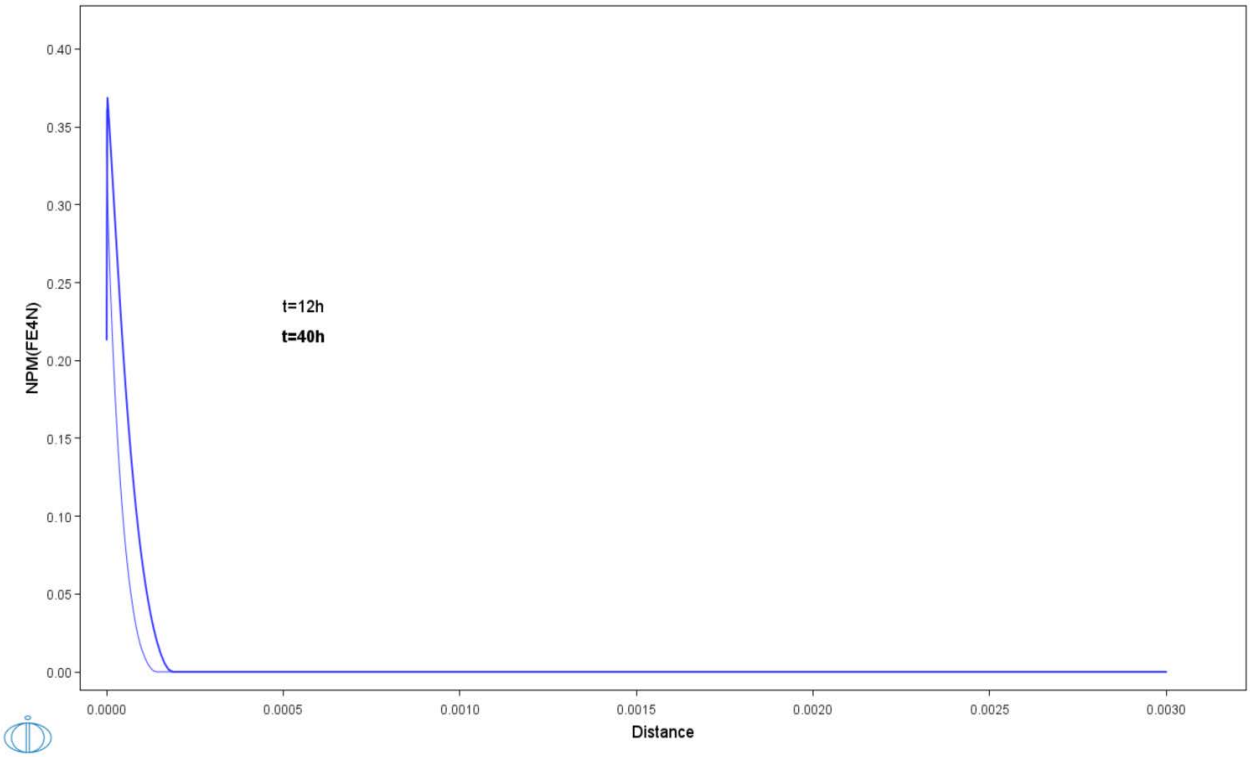

Figure 4.5.3 : Distance from surface vs Phase Fraction of γ' phase after 12 and 40 hours for 1% Al.

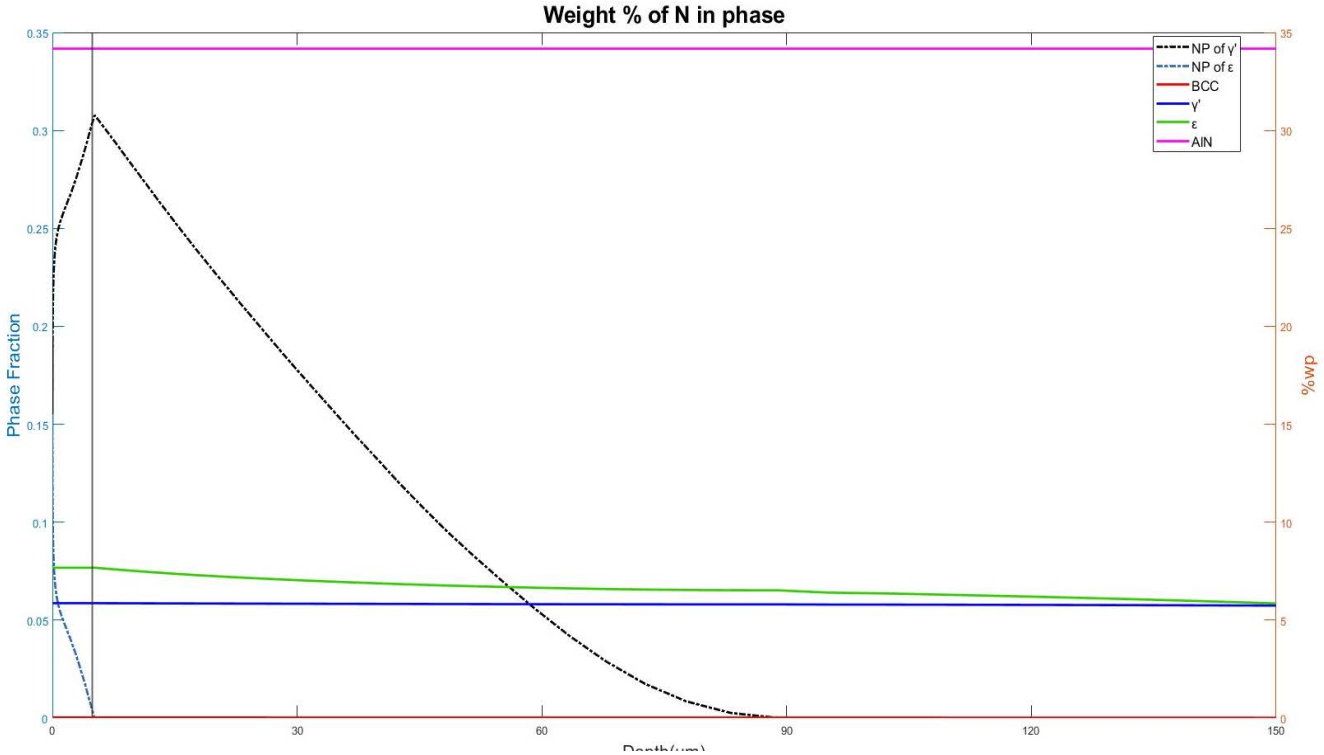

Figure 4.5.4 : Distance from surface vs nitrogen weight percent in phases and Phase Fraction of γ' and ε phases after 40 hours for 1% Al.

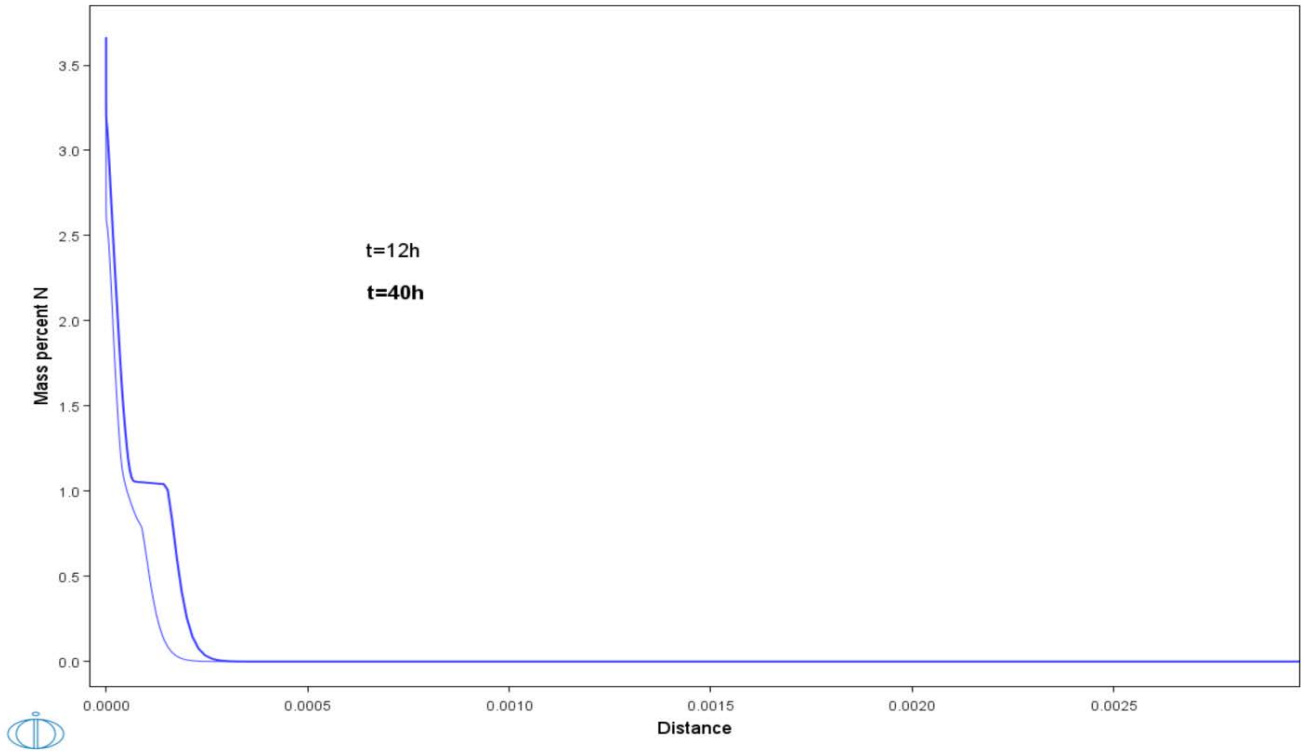

Figure 4.5.5 : Distance from surface vs Weight percent of nitrogen after 12 and 40 hours for 2% Al.

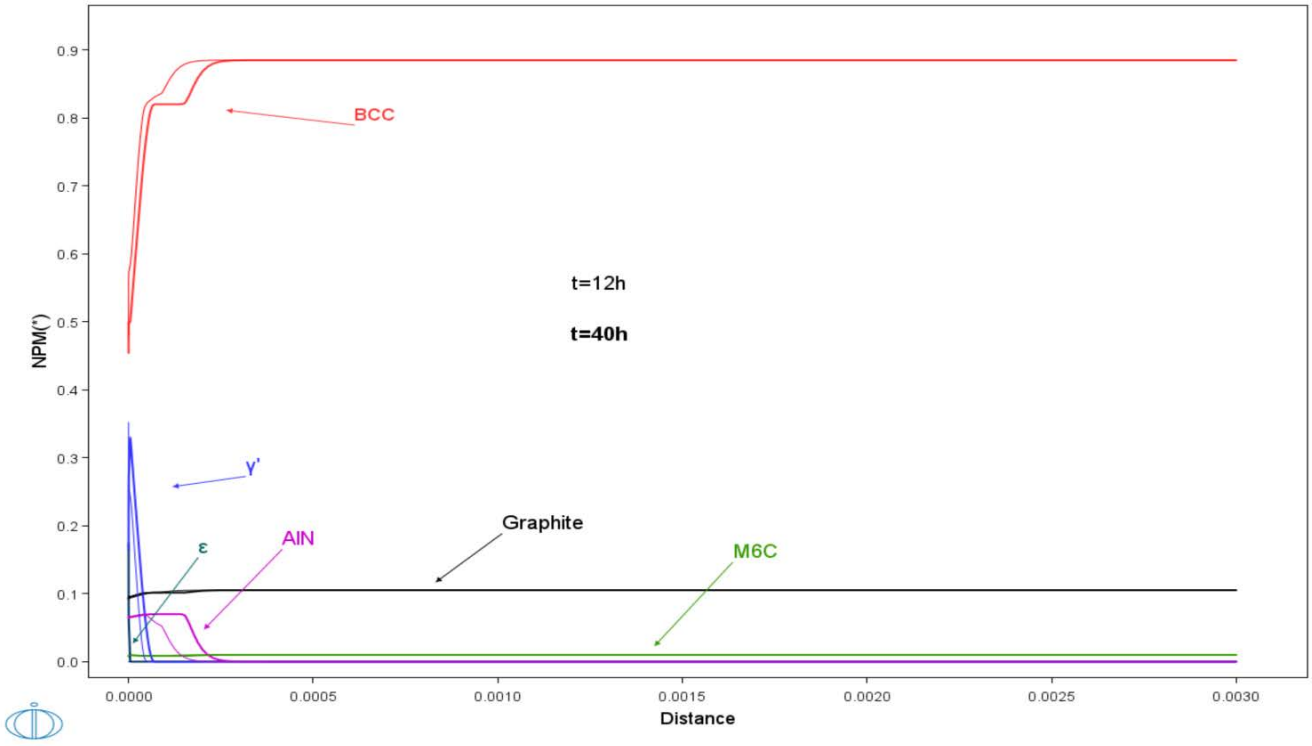

Figure 4.5.6 : Distance from surface vs Phase Fraction of all phases after 12 and 40 hours for 2% Al.

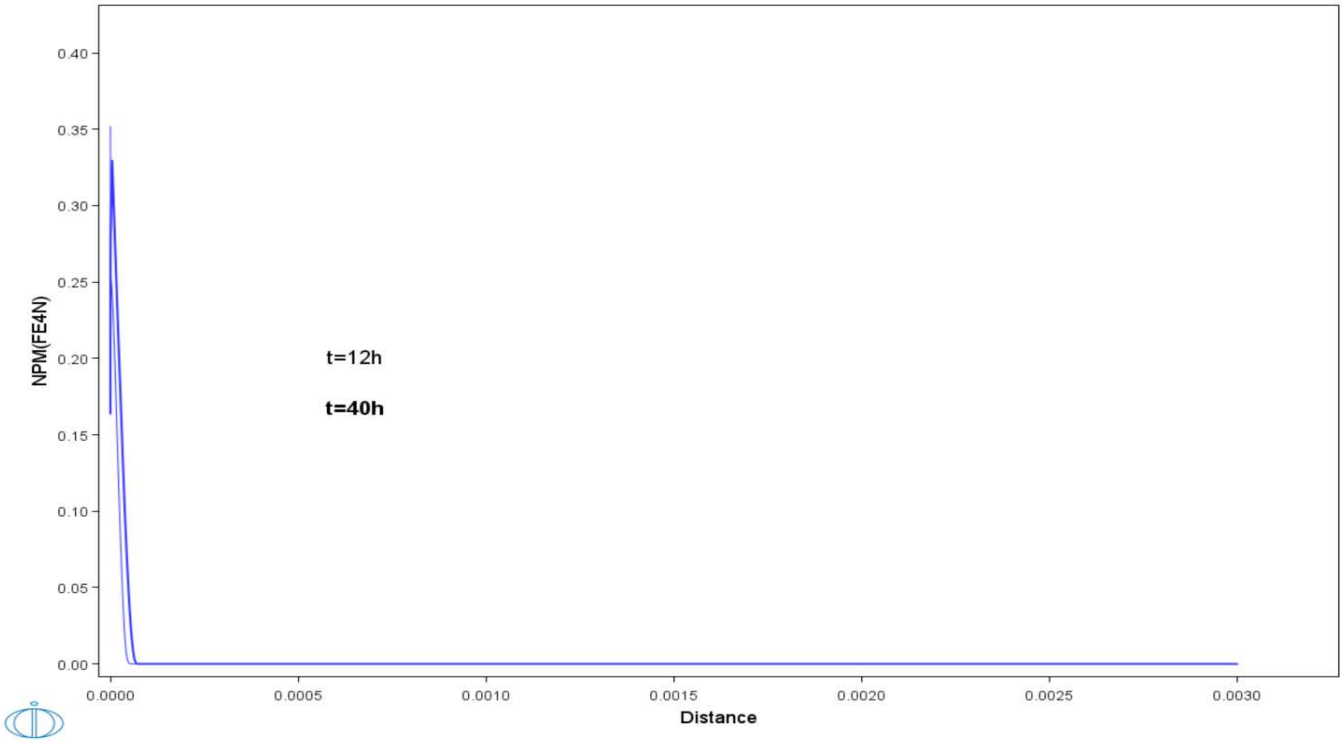

Figure 4.5.7 : Distance from surface vs Phase Fraction of γ' phase after 12 and 40 hours for 2% Al.

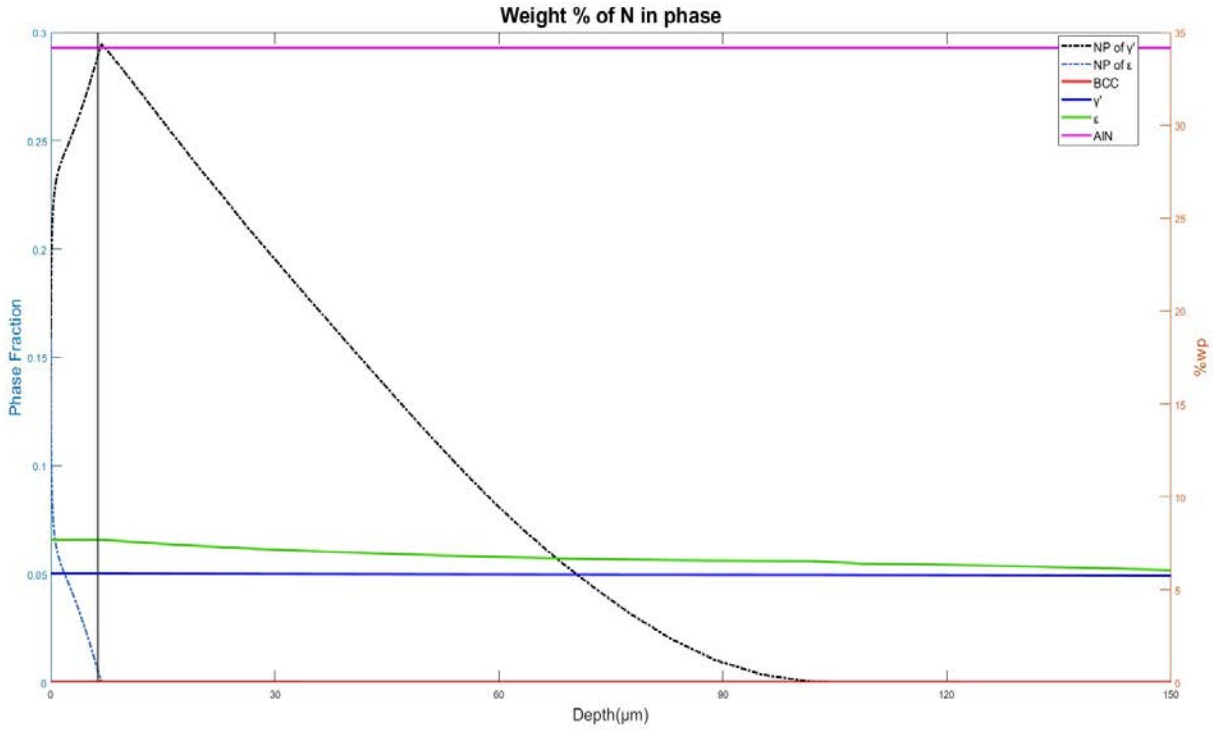

Figure 4.5.8 : Distance from surface vs nitrogen weight percent in phases and Phase Fraction of γ' and ε phases after 40 hours for 2% Al.

Both cases, 1% and 2% Al, have similar response to nitriding with the 0% Al. Again, at time of 12 hours, nitrogen has begun to penetrate to the material reaching peak value of 2.7% and 3% at the surface for 1% and 2% Al correspondingly. At 40 hours, the general picture remains the same as the alloy without aluminum addition. The only major difference is the appearance of AlN phase which absorbs specific amount of nitrogen based on the aluminum content. Analytical numbers for nitriding depth and peak values for phase fractions and nitrogen content will be presented on *Table 4.5.1* at the end of the paragraph. The figures to follow present the data extracted from the simulations for Fe-3.5wt%C–4%Si–1%W-3%Al and Fe-3.5wt%C–4%Si–1%W-4%Al.

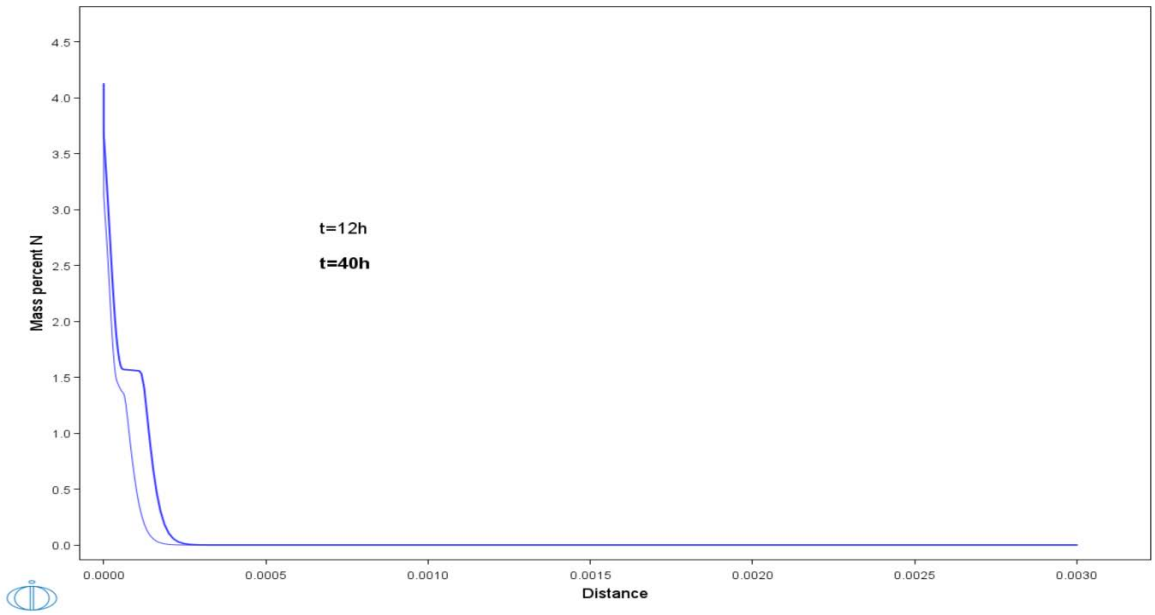

Figure 4.5.9 : Distance from surface vs Weight percent of nitrogen after 12 and 40 hours for 3% Al.

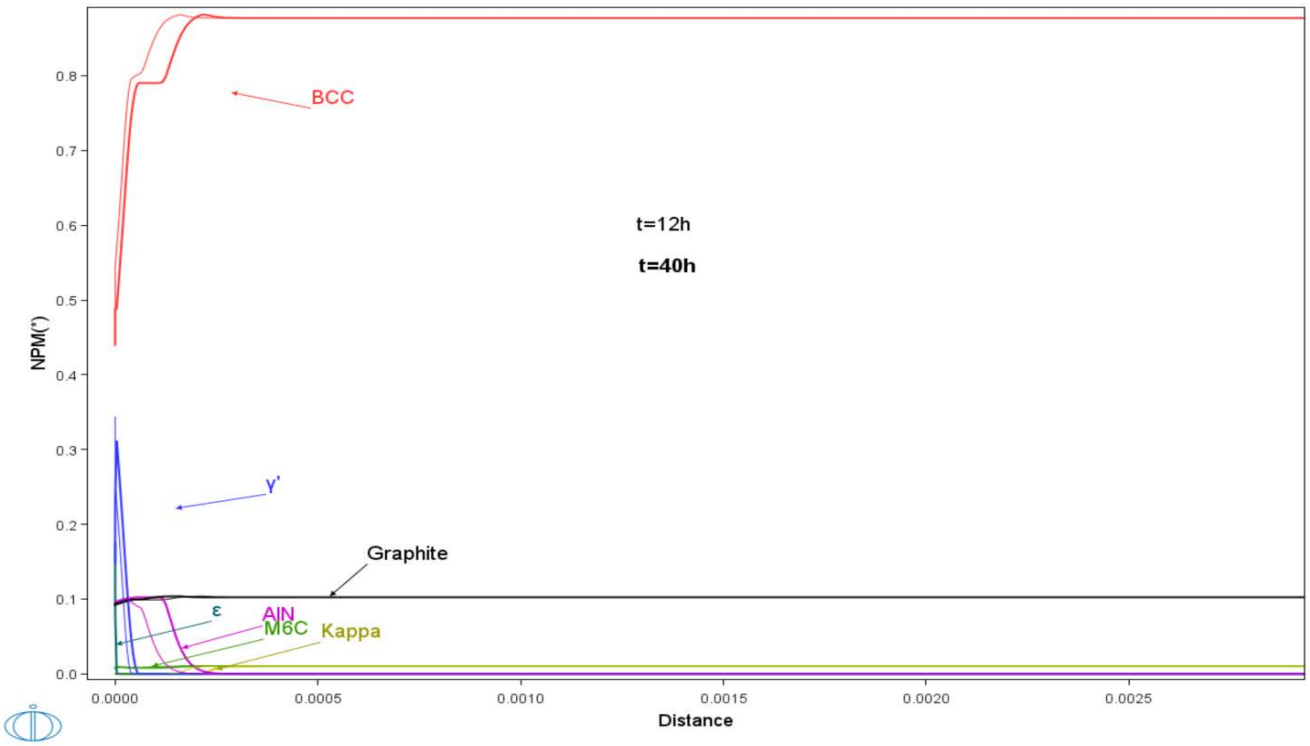

Figure 4.5.10 : Distance from surface vs Phase Fraction of all phases after 12 and 40 hours for 3% Al.

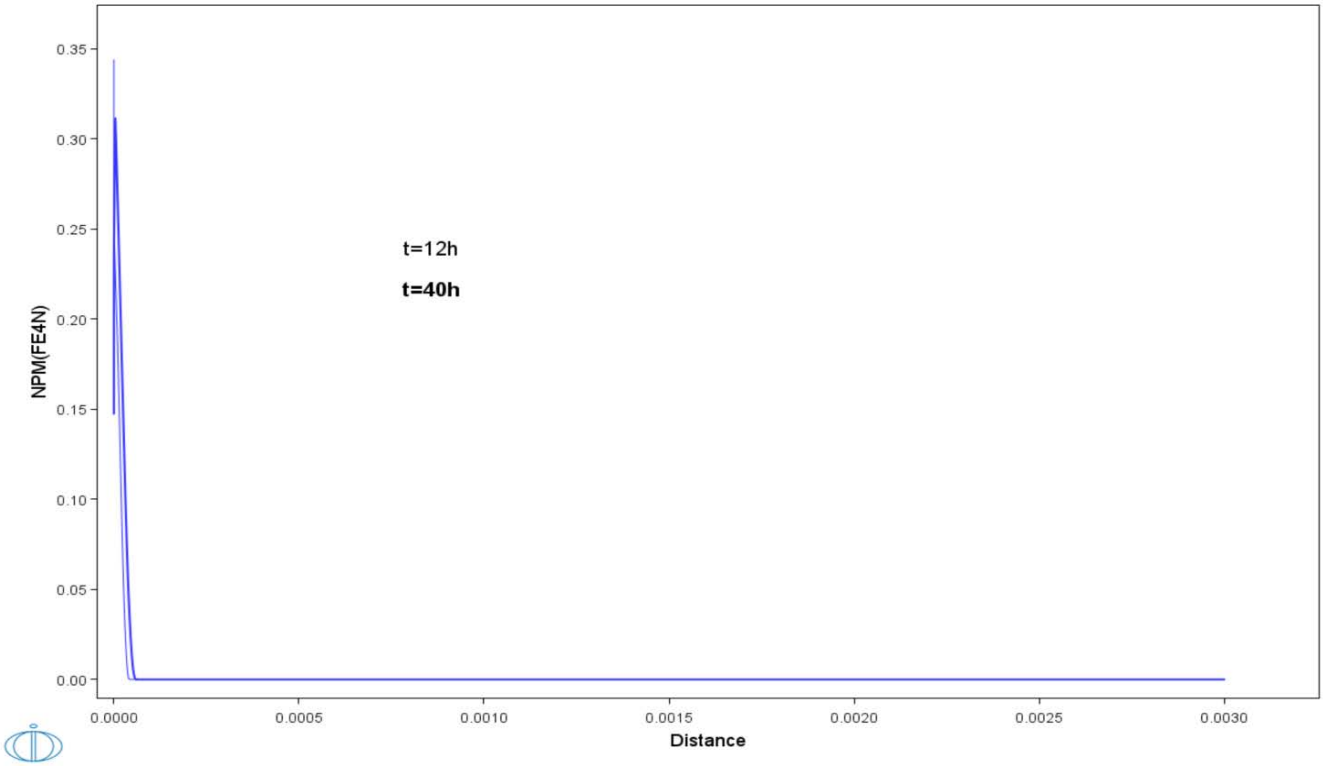

Figure 4.5.11 : Distance from surface vs Phase Fraction of γ' phase after 12 and 40 hours for 3% Al.

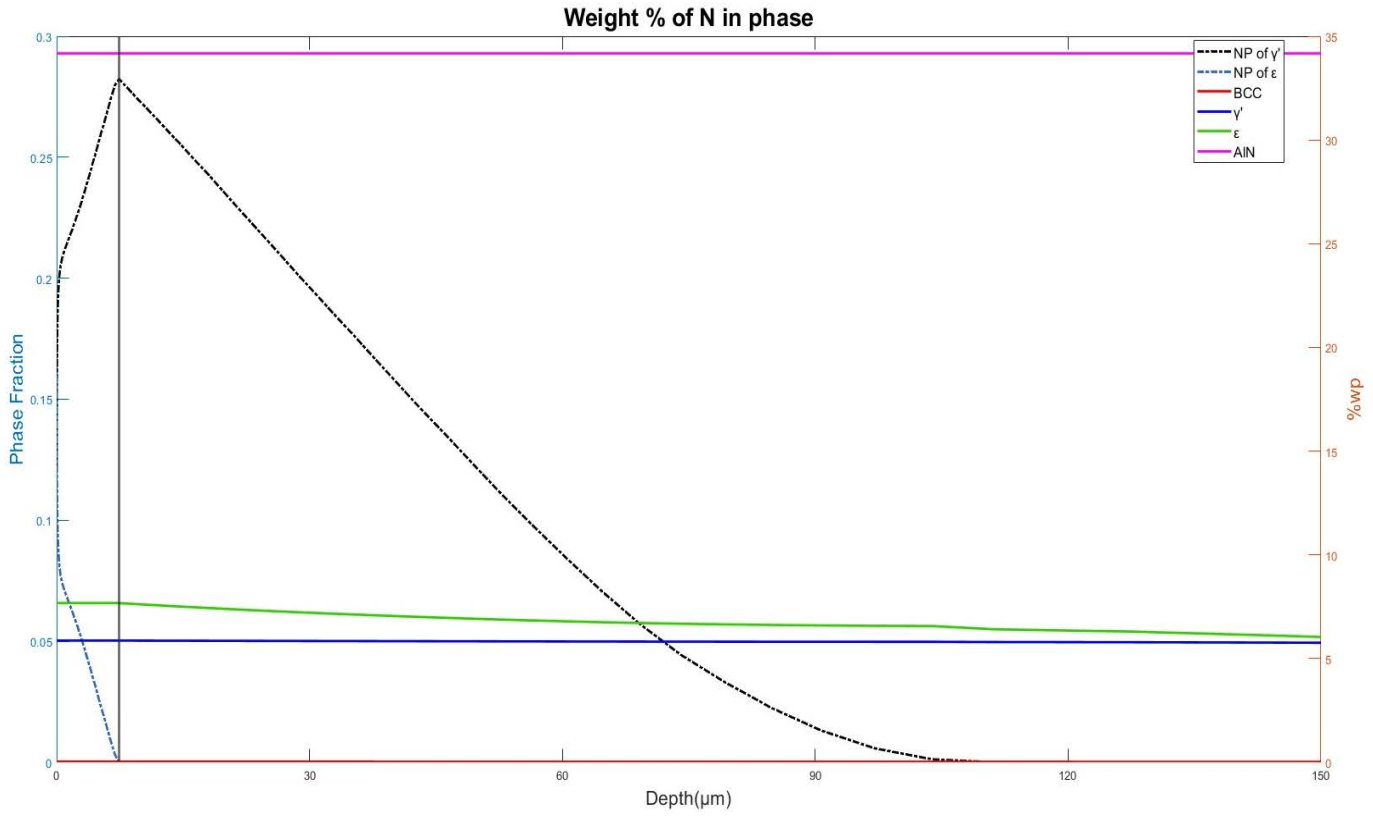

Figure 4.5.12 : Distance from surface vs nitrogen weight percent in phases and Phase Fraction of γ' and ε phases after 40 hours for 3% Al.

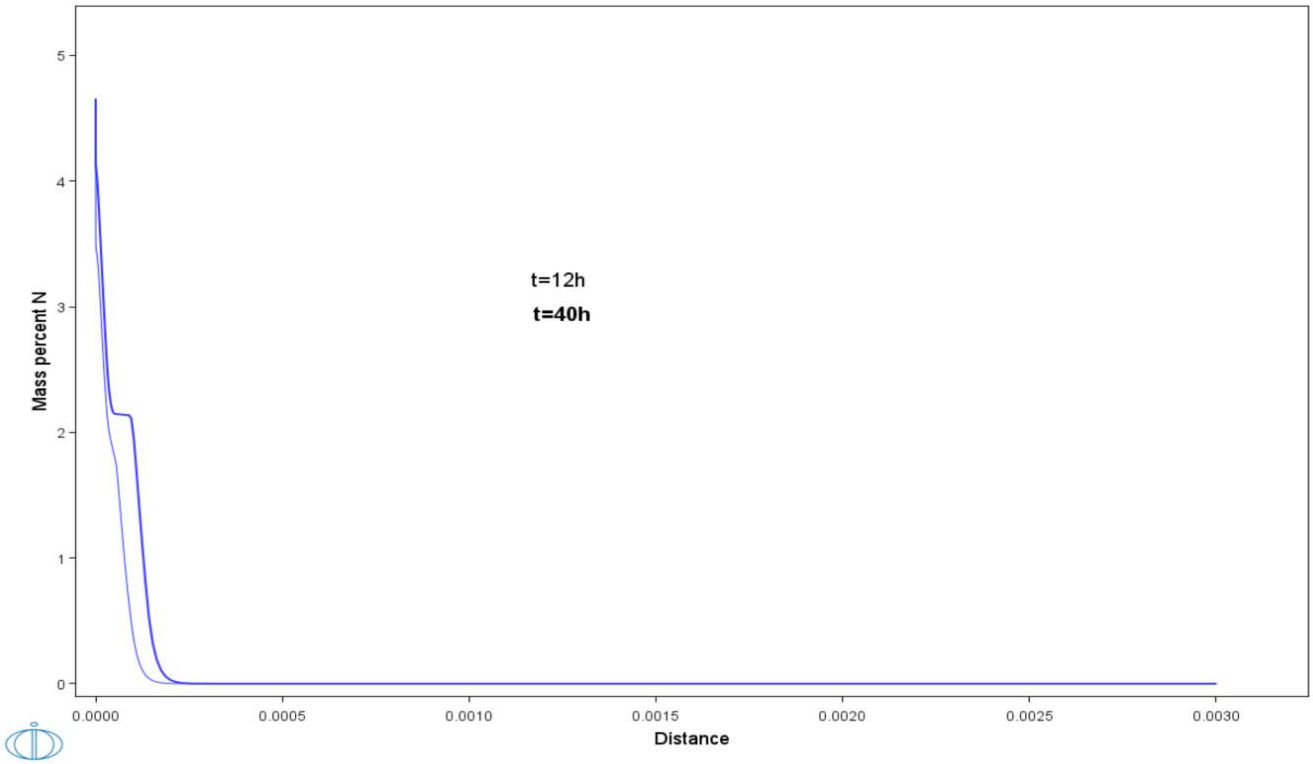

Figure 4.5.13 : Distance from surface vs Weight percent of nitrogen after 12 and 40 hours for 4% Al.

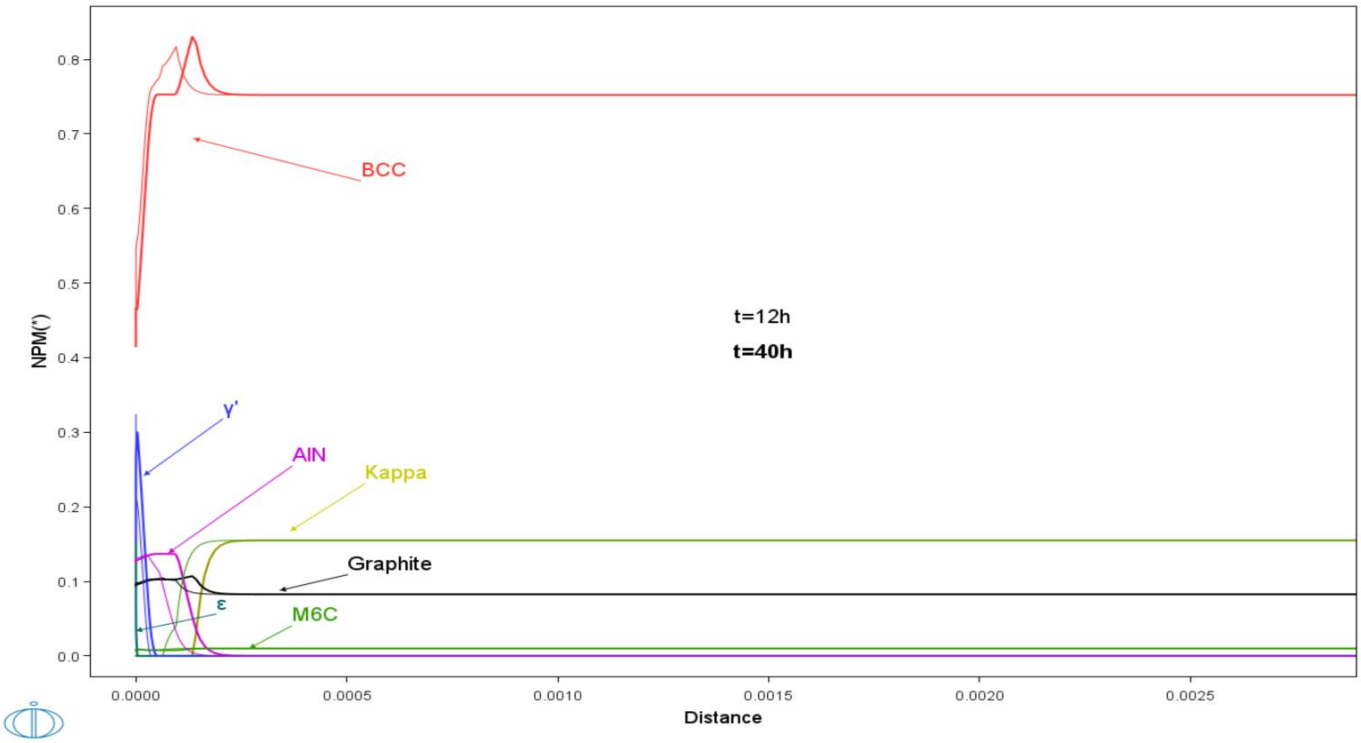

Figure 4.5.14 : Distance from surface vs Phase Fraction of all phases after 12 and 40 hours for 4% Al.

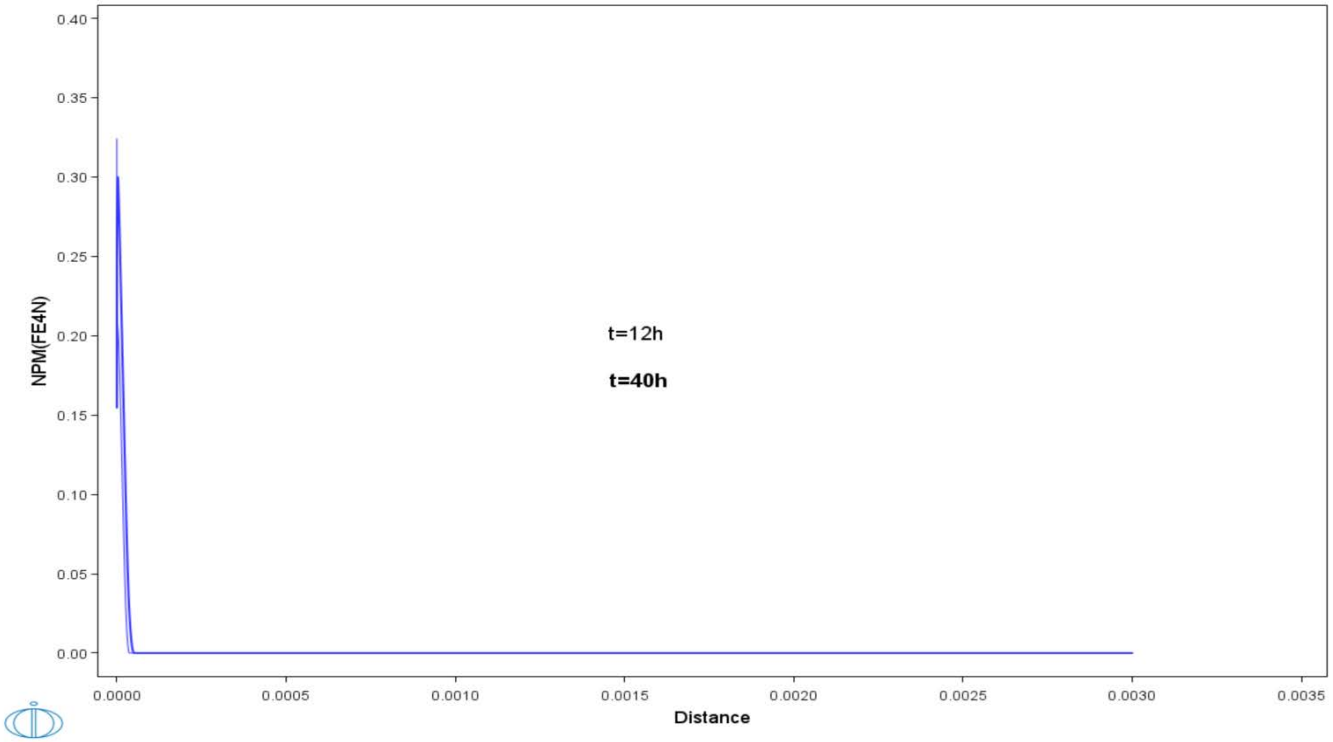

Figure 4.5.15 : Distance from surface vs Phase Fraction of γ' phase after 12 and 40 hours for 4% Al.

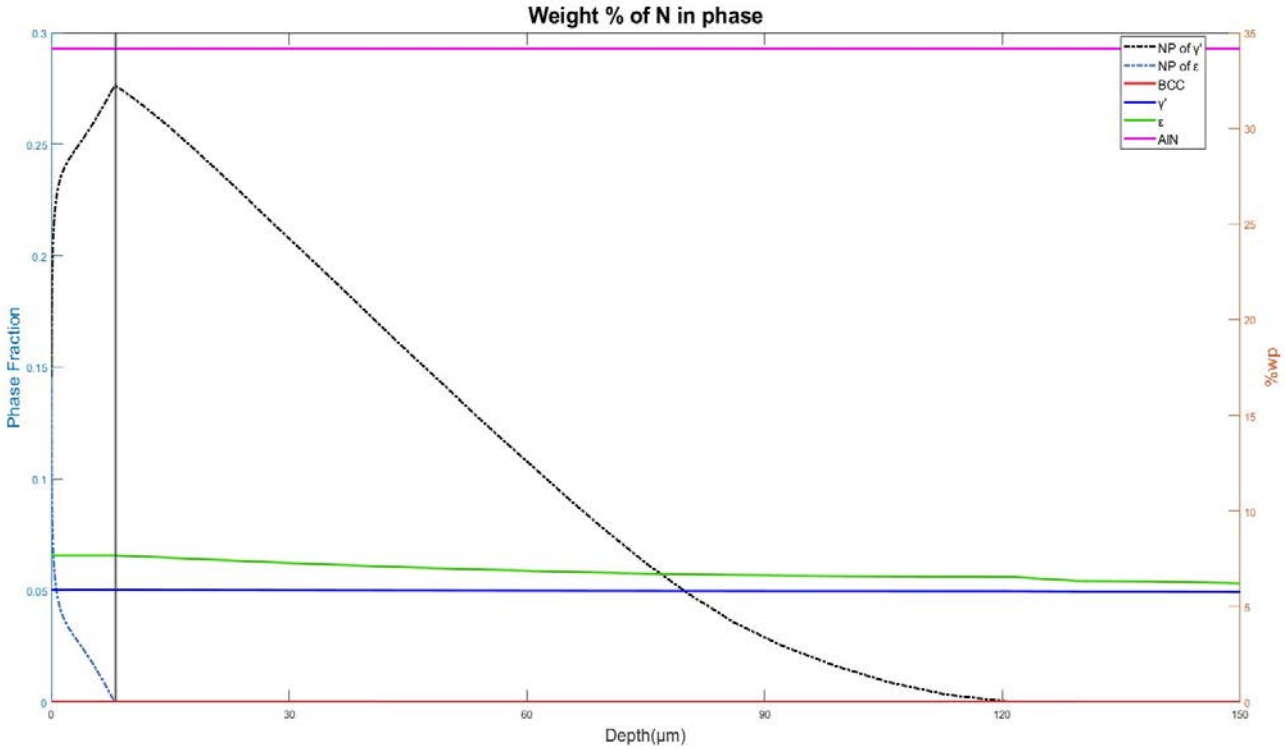

Figure 4.5.16 : Distance from surface vs nitrogen weight percent in phases and Phase Fraction of γ' and ε phases after 40 hours for 4% Al.

Figures *Figure 4.5.9* to *Figure 4.5.16* follow the trend; nitriding is effective further from the surface while ε phase also is pushed inner with extra addition of aluminum. It is worth mentioning that again a new phase appears in relative with the previous alloys, Kappa, that seems to have no impact on the nitriding process and resulting microstructure as it only appears in depths where nitrogen contents drop to zero. Similarly to 1% and 2% data, peak values and nitriding effective depth is presented on *Table 4.5.1* to follow.

Al content	*0%*	*1%*	*2%*	*3%*	*4%*
Max depth of ε	3 μm	8 μm	10 μm	10 μm	12 μm
Max depth of γ'	75 μm	80 μm	100 μm	105μm	120 μm
Max fraction of γ'	32%	31%	30%	28%	28%
Max nitrogen wp%	2.6%	3.25%	3.75%	4.2%	4.6%

Table 4.5.1 : Comparison of different parameters for 0%, 1%, 2%, 3% and 4% Al.

4.6 Effect of Temperature: Simulating at 520°C

Studying the effect of the aluminum addition, led to conclude that higher content boosts nitriding of this cast iron. For this reason, it was decided to focus the rest calculations and research on the alloy containing Fe-3.5wt%C–4%Si–1%W-4%Al. As mentioned in previous

chapters, low temperature nitriding process is usually conducted at a temperature between 500°C and 550°C . It is worth having a sensitivity analysis for nitriding temperature and studying the impact of a relatively small change in temperature. A temperature delta of 10°C was chosen as it is expected to have resulting microstructure enough differentiated to indicate the trend of temperature increment. Also, higher temperatures were avoided as *Figure 3.4.5* thermodynamic calculations contain Liquid phase at higher nitrogen concentrations that may lead to unrealistic results when simulating diffusion. *Figure 4.6.1* to 4.6.3 show the data of the simulation for nitriding at 520°C.

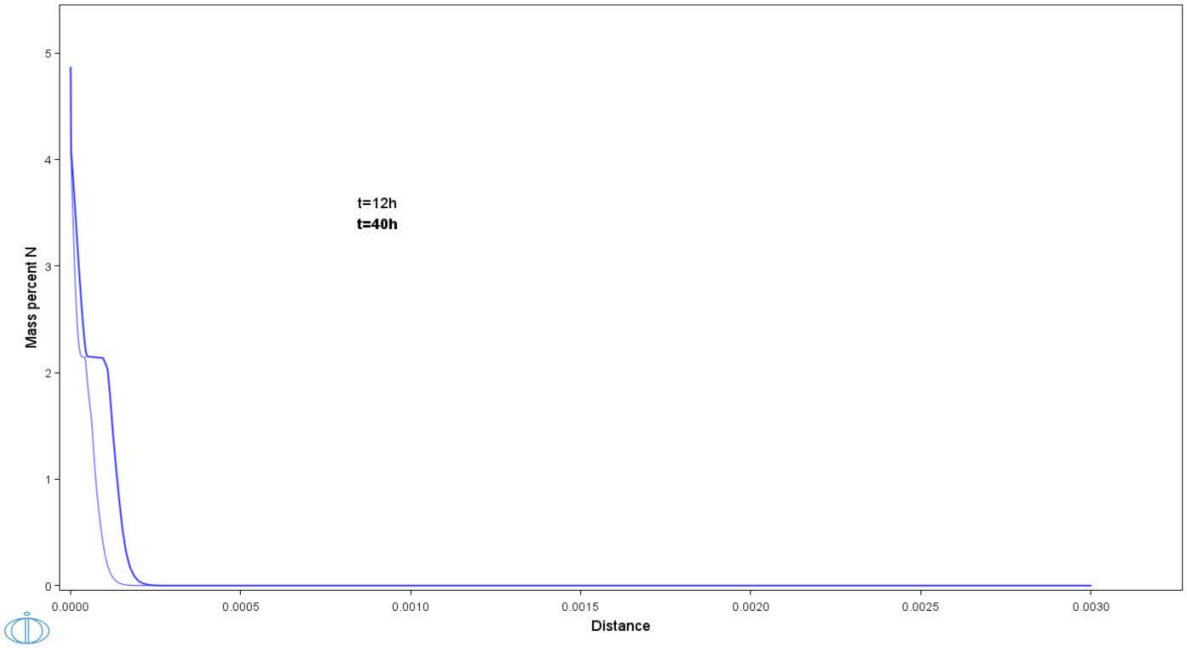

Figure 4.6.1 : Distance from surface vs Weight percent of nitrogen after 12 and 40 hours for 4% Al at 520°C.

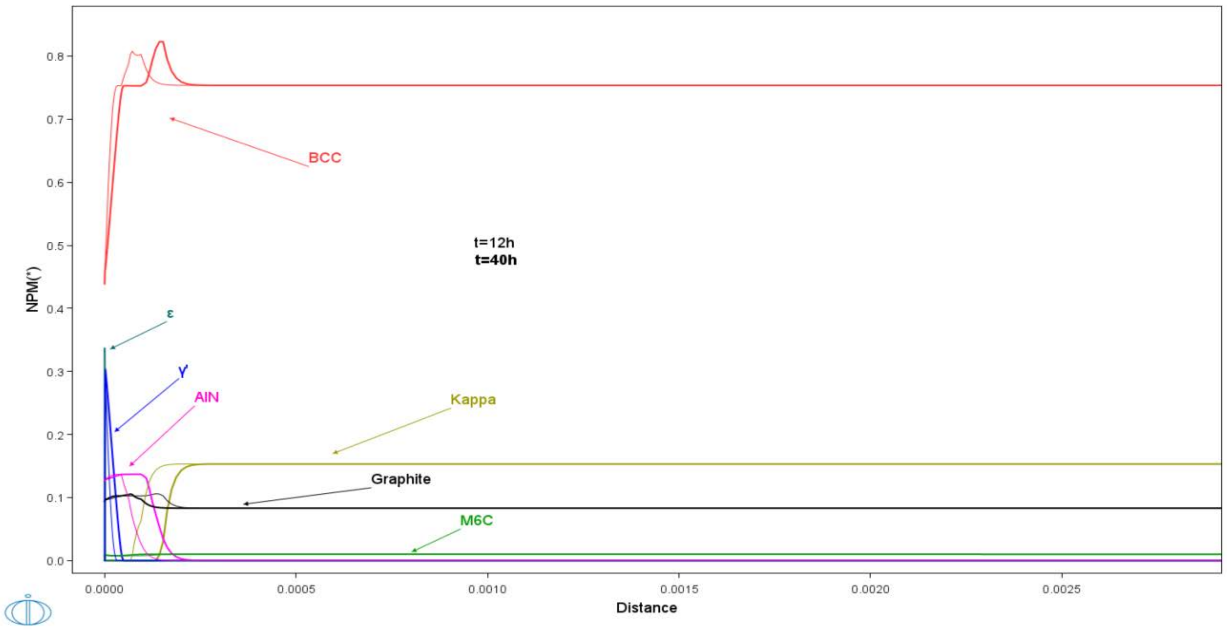

Figure 4.6.2 : Distance from surface vs Phase Fraction of all phases after 12 and 40 hours for 4% Al at 520°C.

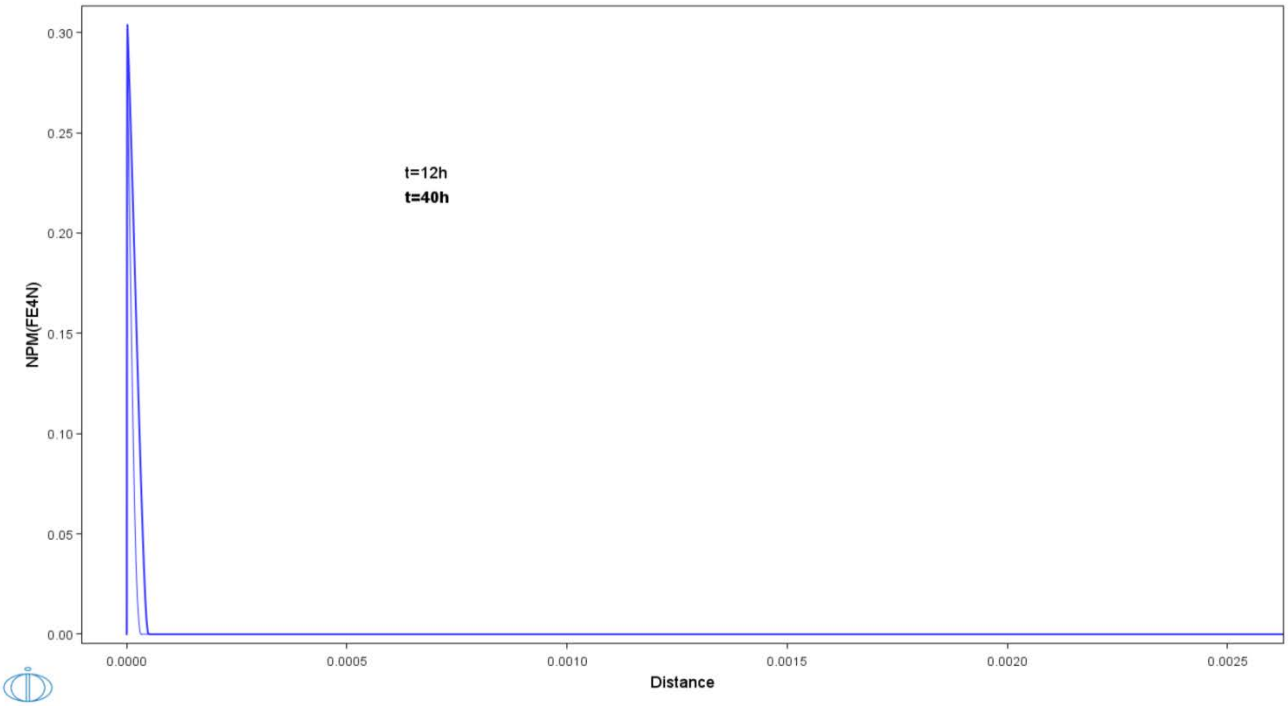

Figure 4.6.3 : Distance from surface vs Phase Fraction of γ' phase after 12 and 40 hours for 4% Al at 520°C.

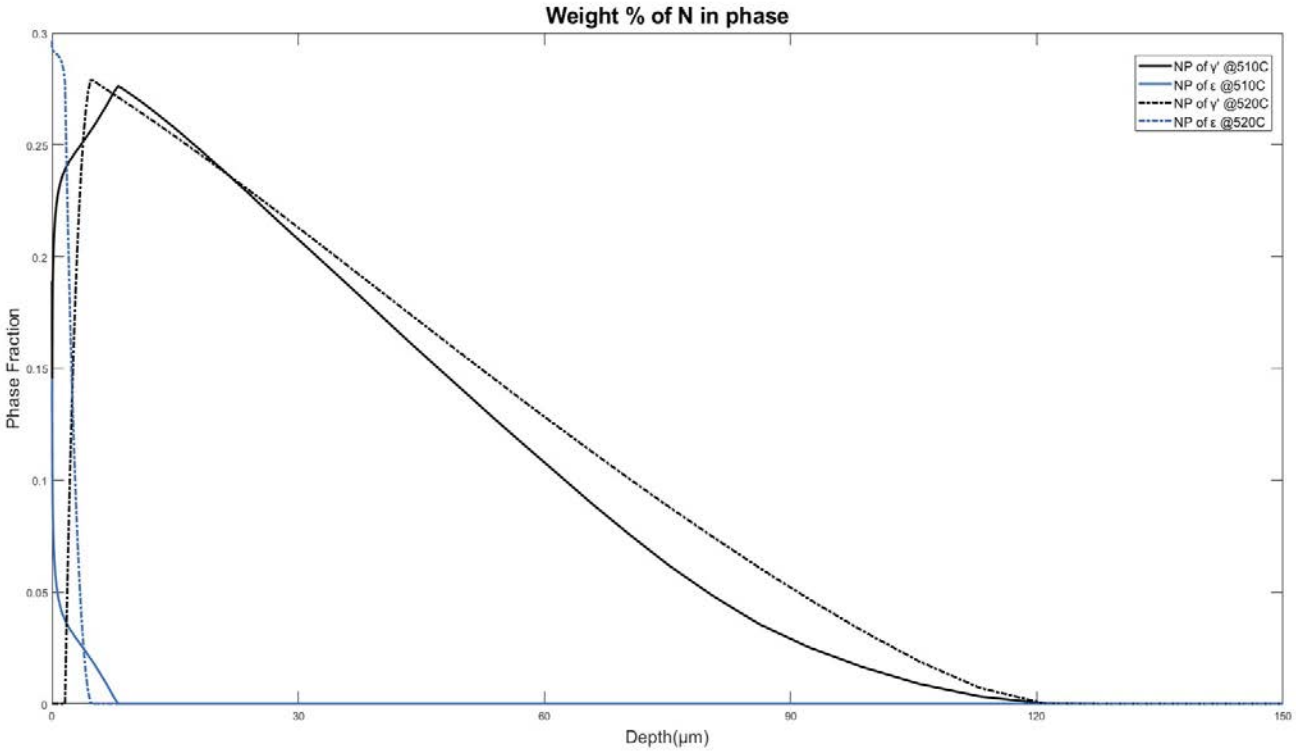

Figure 4.6.4 : Distance from surface vs Phase Fraction of γ' and ε phases after 40 hours for 4% Al comparison for 510°C and 520°C.

Nitriding at higher temperatures seems to push the process even more. Peak nitrogen content reaches 4.9% compared to 4.6% near the surface. However, rise in temperature has a greater impact in the formation of ε and γ' phases. *Figure 4.6.4* compares the distribution of the

two phases for nitriding at 510°C and 520°C. Solid curves correspond to 510°C while dashed and dotted lines account for nitriding at 520°C. Phase γ' even though it has not any major differences in terms of maximum phase fraction and effective depth, has a small shift in the curve. The formation of this phase starts some μm from the surface while maximum phase fraction appears at smaller distance (~5μm) and tends to maintain a bit higher values before it drops to zero. The Delta of 10°C impacts more the formation of ε phase as it pushes the phase into higher fractions with maximum 0.295 maintaining it relatively constant until it drops to zero at 8 μm, 4 μm shorter compared to the lower temperature nitriding. There is no remarkable difference at the maximum depth that γ' phase reaches.

4.7 Simulation for act(N)= 100

An important parameter when setting the kinetic simulation of the model on DICTRA module is the activity for the flux of the nitrogen. There is not a standard value to use as activity for diffusion, so to choose a suitable value there must be some kind of trial and error and choose what seems to be more realistic according to expectations or what better matches some experimental data to produce more result based on the model set. Activity may impact severely the simulation results as it represents the tendency of the nitrogen atoms to "jump" from interstitial-to-interstitial spot. Zero activity means no further migration of nitrogen atoms so basically no diffusion. Augmenting activity equals making the nitriding effect greater; however, this comes to a plateau where the results tend to approach some microstructure no matter how big the activity becomes. For the calculations that preceded, zero flux was chosen for each alloying element of Fe-3.5wt%C–4%Si–1%W-xAl-N except from nitrogen where Activity was set to 500. That value was chosen as it best fitted the available experimental data and helped to set a model capable of producing realistic results for processes that data are not available.

The calculations to follow, explore the differences on simulation resulting microstructure when altering the activity of nitrogen. For this reason, model with act(N)=100 was chosen to be simulated. Expectations are that nitriding will be less intense with reduced nitriding depth and nitrogen content as well as decreased ε, γ' phase fractions and formation depths. Figures to follow reveal how a decrease in activity also changes the microstructure.

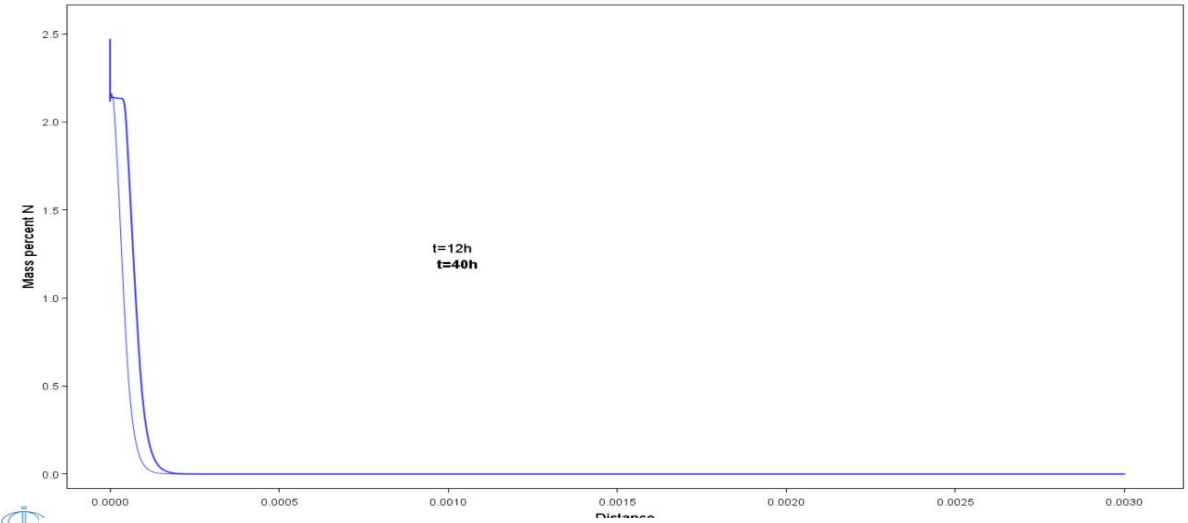

Figure 4.7.1 : Distance from surface vs Weight percent of nitrogen after 12 and 40 hours for 4% Al for Act(N)=100

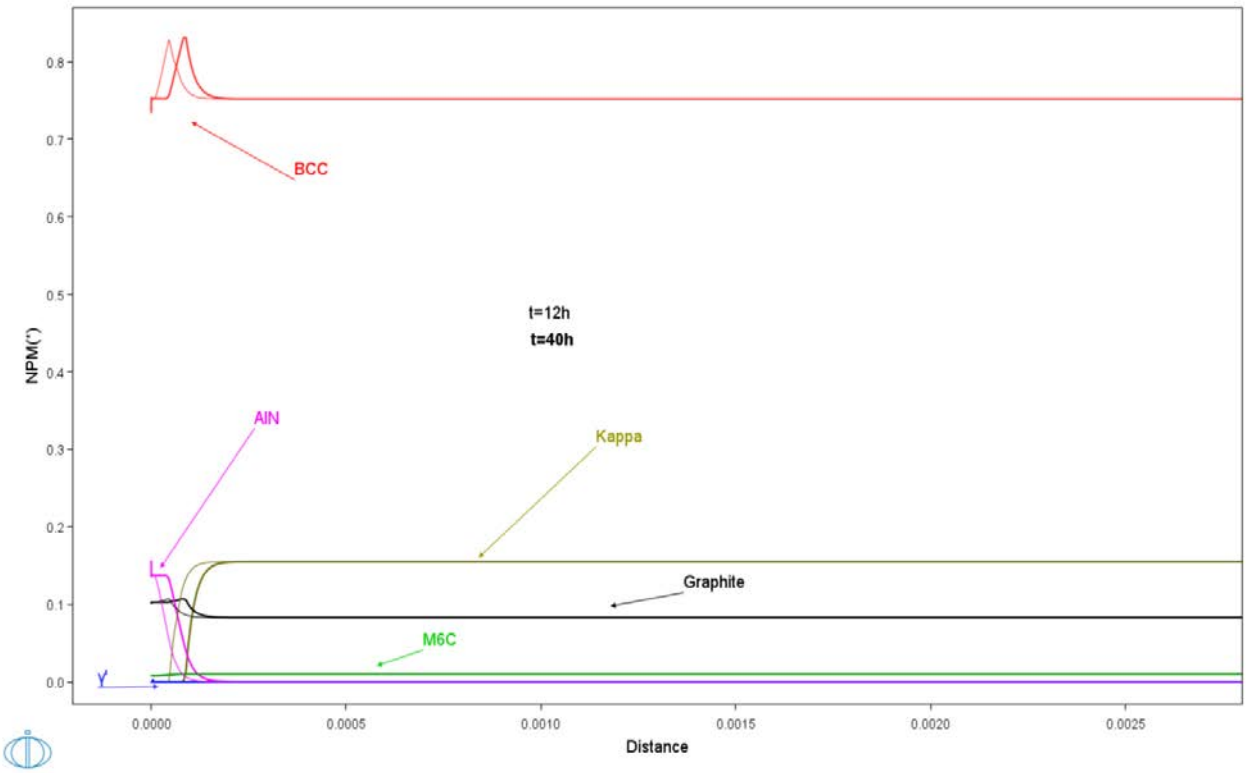

Figure 4.7.2 : Distance from surface vs Phase Fraction of all phases after 12 and 40 hours for 4% Al for Act(N)=100.

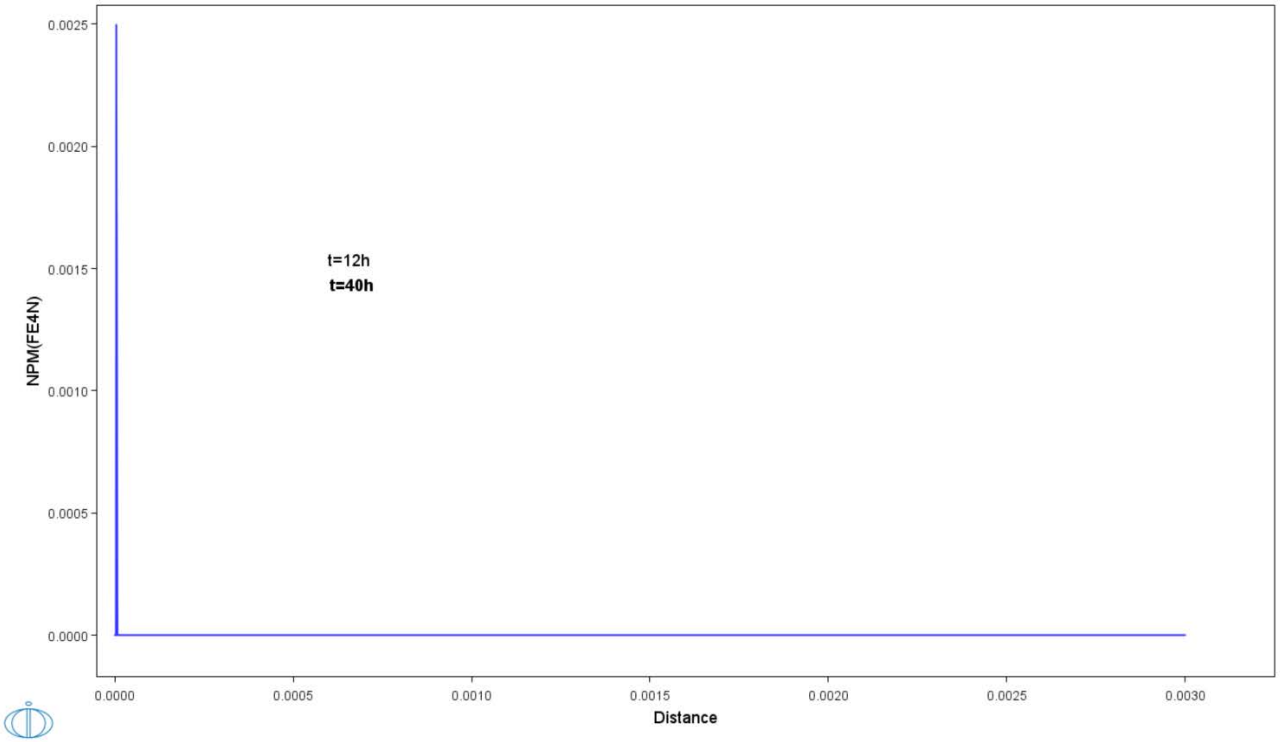

Figure 4.7.3 : Distance from surface vs Phase Fraction of γ' phase after 12 and 40 hours for 4% Al for Act(N)=100.

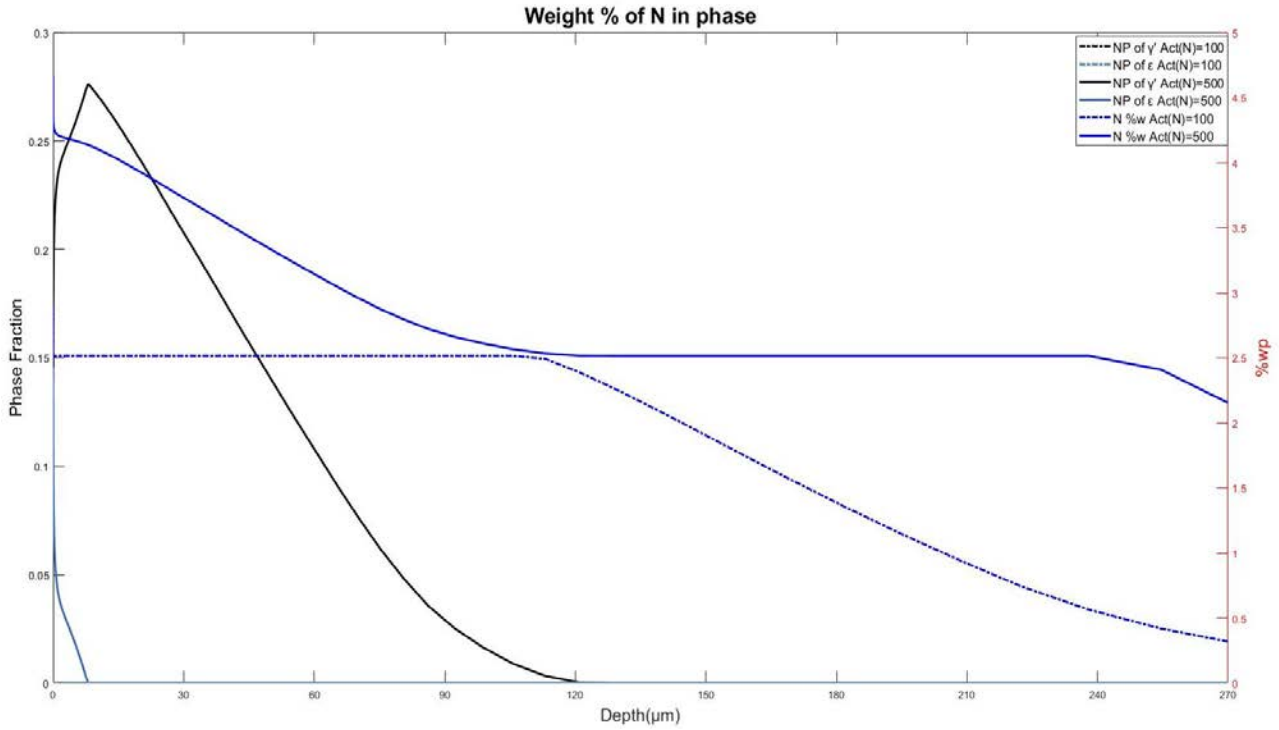

Figure 4.7.4 : Distance from surface vs Phase Fraction of γ' and ε phases after 40 hours for 4% Al comparison for Act(N)=100 and for Act(N)=500.

As expected, this difference in activity has changed the resulting microstructure and the effect of the nitriding is minimal. With activity for nitrogen set at 100, there is no point in making quantity comparisons, because in terms of quality γ' and ε phases are not even forming. Phase ε is completely absent from the calculation results where phase γ' is also practically zero as seen from *Figure 4.7.2*, *Figure 4.7.3* and *Figure 4.7.4*. The only quantity to compare is Nitrogen maximum content and depth; for act(N)=500 nitrogen peaks at 4.6% near the surface where for act(N)=100 this percentage drops to 2.5%. Moreover, for act(N)=500 starts to drop after 270 μm in contrast to act(N)=100 that tends to zero at this point. Consequently, when choosing a model for this process it is wise to use the initial model with act(N)=500 when also referring to the available experimental data.

Chapter 5 : Conclusions

5.1 Thermodynamic Calculations Conclusions

After calculating for equilibrium, the following conclusions emerged:

- Si_3N_4 inhibits the formation of ε phase while it boosts γ' formation. It is of little importance though, because experimental data dictates that this phase should be suppressed.
- Increase of nitrogen content leads to the formation of AlN, ε and γ' phases reducing M_6C, Kappa and α.
- Al addition to the alloy inhibits ε and γ' phases pushing the starting point of their formation to higher nitrogen contents from almost 0.5% for no Al addition to approximately 2.5% for 4% Al. Also, aluminum addition contributes to the appearance of Kappa phase for over 3% Al.

Those calculations not only indicated the resulting microstructure after the process of nitriding but also were adjuvant to set the kinetic DICTRA model.

5.2 Kinetic Simulations Conclusions

When simulating, it was first proposed to work with a realistic model consisting of a compound layer and the diffusion zone. It was concluded after calculations that a model like that could not give reasonable results due to software's incapability and a simpler model should be used. Generally, simulations have shown that there is a direct link between nitrogen percentage of the thermodynamic phase diagrams and the distance from the surface in the kinetic calculations but inversed. After simulating using this model the following emerged.

When simulating to examine **Al addition effect** it was observed that:

- Increase in Al content boosts nitriding. Effective depth of γ' and ε phases also increases while maximum phase fraction of these phases also increases. Obviously, nitrogen percentage has the same behavior as these phases: higher values and deeper penetration of the cast iron.

When simulating to examine **temperature increase effect** it was observed that:

- A temperature delta of 10°C has a remarkable influence on the resulting microstructure.
- For γ' phase there was a minor shift in the curve with the overall behavior being enhanced in terms of phase fraction.

As mentioned above, the nitrogen activity value is not standard but was selected to correspond to the experimental data. Therefore, simulations were carried out to examine the **effect of activity** values at act(N)=100 and at act(N)=500, providing the following observations:

- When activity was selected to act(N)=500, the simulation results appeared to better match the existing experimental data compared to act(N)=100.

- Comparing the two values, when simulating for act(N)=100 the amount of γ′ phase was almost negligible. Furthermore, ε phase did not form at all.
- At a depth value of 270μm, the nitrogen content was significantly higher for act(N)=500, while it was almost zero for act(N)=100.

Chapter 6 : References

[1] Heywood, J. (2018). Internal Combustion Engine Fundamentals 2E. McGraw-Hill Education.

[2] Reif, K. (2014b). Diesel Engine Management: Systems and Components. Springer.

[3] Tiedje, N. S. (2010). Solidification, processing and properties of ductile cast iron. *Materials Science and Technology*, *26*(5), 505–514. https://doi.org/10.1179/026708310x12668415533649

[4] Celik, O., Ahlatci, H., Kayali, E. S., & Cimenoglu, H. (2004). High temperature abrasive wear behavior of an as-cast ductile iron. *Wear*, *258*(1–4), 189–193. https://doi.org/10.1016/j.wear.2004.09.004

[5] E, I. A., Kelly, O. E., & Abdulsamad, G. (2017). Engineering material selection for automotive exhaust systems using CES software. *International Journal of Engineering Technologies IJET*, *3*(2), 50–60. https://doi.org/10.19072/ijet.282847

[6] Çelik, G., Tzini, M., Polat, Ş., Aristeidakis, J., Atapek, Ş., Sarafoglou, P., & Haidemenopoulos, G. (2021). Simulation and analysis of the solidification characteristics of a Si-Mo ductile iron. *Journal of Mining and Metallurgy Section B Metallurgy*, *57*(1), 53–62. https://doi.org/10.2298/jmmb200717003c

[7] M. Ekström: Development of a Ferritic Ductile Cast Iron for Increased Life in Exhaust Applications, Licentiate Thesis, Royal Institute of Technology, Stockholm, Sweden, 2013, ISBN 978-91-7501-711-2.

[8] Çelik, G. A., Tzini, M. T., Polat, Ş., Atapek, Ş. H., & Haidemenopoulos, G. N. (2020b). Matrix design of a novel ductile cast iron modified by W and Al: A comparison between thermodynamic modeling and experimental data. *Metallurgical and Materials Engineering*, *26*(1), 15–29. https://doi.org/10.30544/449

[9] Çelik, G. A., Atapek, Ş. H., Polat, Ş., & Haidemenopoulos, G. N. (2023). Modelling and characterization of the silicon effect on the oxidation of novel SiNb cast irons. *Journal of Alloys and Compounds*, *977*, 173332. https://doi.org/10.1016/j.jallcom.2023.173332

[10] Routsi M., (2024) , Thermodynamic and Kinetic Analysis of Nitriding in Ductile Cast Iron Fe- 3.4%C- 4%Si- 1%Nb- (0-4) %Al ,Diploma Thesis,Department of Mechanical Engineering, University of Thessaly (Volos).

[11] Bil'chenko, A. V., & Dunaeva, S. A. (1975). Characteristics of nitriding of cast irons. *Metal Science and Heat Treatment*, *17*(12), 1021–1022. https://doi.org/10.1007/bf00664203

[12] G.N. Haidemenopoulos, Physical Metallurgy: Principles and Design, 1st ed., CRC Press, 2018. https://doi.org/10.1201/9781315211220

[13] Nam, N. D., Xuan, N. A., Van Bach, N., Nhung, L. T., & Chieu, L. T. (2019). CONTROL GAS NITRIDING PROCESS: a REVIEW. *Journal of Mechanical Engineering Research and Developments*, *42*(1), 17–25. https://doi.org/10.26480/jmerd.01.2019.17.25

[14] Zhou, Y., Xia, F., Xie, A., Peng, H., Wang, J., & Li, Z. (2023). A Review—Effect of Accelerating Methods on Gas Nitriding: Accelerating mechanism, nitriding behavior, and Techno-Economic Analysis. *Coatings*, *13*(11), 1846. https://doi.org/10.3390/coatings13111846

[15] Kondakci, E., & Solak, N. (2020). The effect of microstructure on nitriding mechanism of cast iron. *International Journal of Metalcasting*, *14*(4), 1033–1040. https://doi.org/10.1007/s40962-019-00404-2

[16] Grün, R., & Günther, H. (1991). Plasma nitriding in industry—problems, new solutions and limits. *Materials Science and Engineering A*, *140*, 435–441. https://doi.org/10.1016/0921-5093(91)90459-z

[17] Berg, M., Budtz-Jørgensen, C., Reitz, H., Schweitz, K., Chevallier, J., Kringhøj, P., & Bøttiger, J. (2000). On plasma nitriding of steels. *Surface and Coatings Technology*, *124*(1), 25–31. https://doi.org/10.1016/s0257-8972(99)00472-7

[18] Bonow, V. T., Maciel, D. S., Fenner, N. L., Reguly, A., Zimmer, A., & Zimmer, C. G. (2021). Nitriding in non-toxic salts bath: An approach to implement cleaner production in the metallurgic industry. *Cleaner Engineering and Technology*, *4*, 100169. https://doi.org/10.1016/j.clet.2021.100169

[19] Somers, M. A. J. (2013). Nitriding and Nitrocarburizing; Current Status and Future Challenges. Paper presented at Heat Treat & Surface Engineering Conference & Expo 2013, Chennai, India.

[20] Atapek, Ş. H., Altin, I., Çelik, G. A., Polat, Ş., Haidemenopoulos, G. N., & Kamoutsi, E. (2024, October). Presented at the 4th International Symposium on Characterization, Sakarya, Turkey.

[21] Çelik, G. A., Tzini, M. T., Polat, Ş., Atapek, Ş. H., & Haidemenopoulos, G. N. (2020a). Thermal and microstructural characterization of a novel ductile cast iron modified by aluminum addition. *International Journal of Minerals Metallurgy and Materials*, *27*(2), 190–199. https://doi.org/10.1007/s12613-019-1876-8

[22] Kattner, U. R. (2016). THE CALPHAD METHOD AND ITS ROLE IN MATERIAL AND PROCESS DEVELOPMENT. *Tecnologia Em Metalurgia Materiais E Mineração*, *13*(1), 3–15. https://doi.org/10.4322/2176-1523.1059

[23] Borgenstam, A., Höglund, L., Ågren, J., & Engström, A. (2000). DICTRA, a tool for simulation of diffusional transformations in alloys. *Journal of Phase Equilibria*, *21*(3), 269–280. https://doi.org/10.1361/105497100770340057

[24] Andersson, J., Helander, T., Höglund, L., Shi, P., & Sundman, B. (2002). Thermo-Calc & DICTRA, computational tools for materials science. *Calphad*, *26*(2), 273–312. https://doi.org/10.1016/s0364-5916(02)00037-8